



## Sedimentary stacking pattern of plastered drifts: An example from the Cenozoic on the Uruguayan continental slope

Kirby A.<sup>a,\*</sup>, F.J. Hernández-Molina<sup>a</sup>, P. Rodríguez<sup>b</sup>, B. Conti<sup>b</sup>

<sup>a</sup> Department of Earth Sciences, Royal Holloway University of London, Egham, Surrey TW20 0EX, UK

<sup>b</sup> ANCAP, Exploración y Producción, Paysandú s/n esq. Av. del Libertador, 11100 Montevideo, Uruguay

### ARTICLE INFO

#### Keywords:

Deep-water sedimentation  
Contourites  
Plastered drifts  
Continental margin  
Cenozoic  
Uruguay

### ABSTRACT

Plastered drifts are a complex type of contouritic drift, very common along continental slopes, although their precise sedimentary stacking pattern and long-term evolution are not well understood. In this work we used 3D and 2D multichannel reflection seismic and well datasets to characterize a Paleogene plastered drift along the Uruguayan continental margin. A large buried drift running parallel to the middle and lower slope was identified, comprising five main seismic units (SU1-SU5) and a number of subunits subdivided by internal widespread erosive discontinuities. An extensive contourite terrace is developed on the landward top of the drift, while smaller-scale bottom current features (channels and bedforms) denote a hierarchy of features related to water mass circulation and interfaces, as well as associated oceanographic processes. Four long-term evolutionary stages were decoded in the plastered drift formation: I) *Onset Stage* (66 Ma – 56 Ma), whose basal surface represents a prominent erosional surface marking the onset of drift, after which extensive sheeted deposits develop; II) *Growth Stage* (Eocene ~ 56 – ~38 Ma) with a prominent *backstepping* sedimentary stacking pattern; III) *Maintained Stage* (~38 Ma – ~20 Ma) of limited growth of the drift, characterised by aggradational sheeted deposits and extensive erosion; and IV) *Burial Stage* (<20 Ma), which determines a major change in the margin evolution—the main depocenter shifts to deeper domains, leading to the final burial of the drift. The plastered drift formation is attributed to the influence of a deeper and weak water mass and a shallower but more vigorous water mass, as well as their interface. The aforementioned evolutionary stages and the greatest changes in the drift depositional style would be a consequence of spatial and vertical changes in these water masses over millions of years, the Growth Stage being related to the expansion and intensification of deep-water circulation that modulated the formation of the proximal terrace at its top and resulted in the *backstepping* stacking pattern. The smaller lateral and vertical changes in the seismic units and subunits along the drift are linked to local bottom current processes and their interaction with the slope morphology, the slope gradient playing a key role in the lateral bottom current behavior. This study shows the complex lateral and temporal sedimentary stacking pattern and evolution of a contouritic drift, and decodes the dominant oceanographic and depositional processes in its long-term formation. In doing so, we demonstrate the requirement of extensive 2D and 3D seismic datasets for accurate characterisations. Still, similar research in other continental margins is needed to better understand how and when (in geological time) large contouritic drifts are generated, in light of their implications for basin analysis, paleoceanographic reconstructions, and energy geosciences.

### 1. Introduction

The term ‘contourite’ refers to a spectrum of sediments deposited or substantially reworked by the persistent action of bottom currents (e.g., Stow et al., 2002; Rebesco and Camerlenghi, 2008; Rebesco et al., 2014). Bottom currents interact with the seafloor to generate large depositional (“drift”), erosional and mixed contourite features, which are prominent

and common along continental margins and on abyssal plains (Faugères and Stow, 1993; Faugères et al., 1999; García et al., 2009; Preu et al., 2013; Rebesco et al., 2014; Hernández-Molina et al., 2016, 2018; Thiéblemont et al., 2019; Rodrigues et al., 2020, 2021). Such features often develop coevally and may form ‘contourite depositional systems’ (CDS) that evolve laterally and temporally (Hernández-Molina et al., 2003). Recent studies have shown that beyond their economic potential

\* Corresponding author.

E-mail address: [Adam.Kirby.2016@live.rhul.ac.uk](mailto:Adam.Kirby.2016@live.rhul.ac.uk) (A. Kirby).

<https://doi.org/10.1016/j.margeo.2021.106567>

Received 22 March 2021; Received in revised form 30 June 2021; Accepted 12 July 2021

Available online 26 July 2021

0025-3227/© 2021 The Authors.

Published by Elsevier B.V. This is an open access article under the CC BY-NC-ND license

(<http://creativecommons.org/licenses/by-nc-nd/4.0/>).

(Viana, 2008; Fonesu et al., 2020), contourites are crucial for paleoceanographic and environmental reconstructions (Rebesco et al., 2014; Lofi et al., 2016). Moreover, the increased availability of regional high resolution two-dimensional (2D) and three-dimensional (3D) seismic data has led to the more widespread identification of such deposits and in greater detail than ever before (e.g. Sun et al., 2017; Yin et al., 2019; Miramontes et al., 2019; Thiéblemont et al., 2020; Fonesu et al., 2020). Despite advances, the criteria for interpreting large contourite features in seismic data (Faugères et al., 1999; Rebesco, 2005; Nielsen et al., 2008; Hernández-Molina et al., 2008a, 2008b; Rebesco et al., 2014) call for revision, including some drifts not fully clarified or missing from current classifications. In addition to their primary features, smaller secondary features are being determined (e.g., Preu et al., 2013; Thiéblemont et al., 2019; Yin et al., 2019; Miramontes et al., 2020) and associated with secondary oceanographic processes (e.g. internal solitary waves/tides, cores, vertical eddies and horizontal vortices) that may influence CDS.

One common type of large contouritic drift is the plastered drift, originally described by McCave and Tucholke (1986) and Faugères et al. (1999) and the recent focus of substantial research (Preu et al., 2013; Hernández-Molina et al., 2018; Miramontes et al., 2019; Thiéblemont et al., 2019; Rodrigues et al., 2020). They show an overall convex geometry, with sediment accumulating towards the centre, at any depth along continental slopes, yet most often in conjunction with a gentle slope and weak bottom current (Faugères et al., 1999; Faugères and Stow, 2008). Their seismic units typically have a broad shallowly mounded geometry of little apparent migration, though internal gently downlapping reflections might indicate slight down-current progradation that could have an obliquely landward or basinward element, while the internal facies are typically low amplitude to transparent discontinuous reflections (Faugères et al., 1999; Miramontes et al., 2019). Such features are elongated parallel to the slope, showing

upslope or down-slope migration (Faugères et al., 1999; Rebesco, 2005). Plastered drifts may be genetically related to other erosive or depositional features such as terraces, contourite channels (or moats), or sedimentary waves (Rodrigues et al., 2020; Thiéblemont et al., 2020) resulting in a large CDS (Hernández-Molina et al., 2003; Hernández-Molina et al., 2006). Recent studies have hinted at the underlying complexity of plastered drift evolution and enhanced their classification (e.g. Hernández-Molina et al., 2009, 2018; Preu et al., 2013; Thiéblemont et al., 2019; Miramontes et al., 2020; Rodrigues et al., 2020), despite this, further research is needed to elucidate the vertical and lateral changes in their sedimentary stacking pattern and shape.

Using a combination of 2D and 3D seismic reflection datasets, this study aims to determine sedimentary and oceanographic processes responsible for the development of a large plastered drift preserved below the Uruguayan slope (Fig. 1). This is achieved by decoding complex lateral and vertical changes in its sedimentary stacking pattern. The research contributes to the growing body of knowledge of how these large depositional features form, and demonstrates the utility 3D seismic reflection data in the study of CDSs.

## 2. Geological setting

The Uruguayan Margin is a segmented, volcanic rifted margin (Fig. 1) located between 33°S and 38°S on the east coast of South America and covering an area of approximately 130,000 km<sup>2</sup> (Soto et al., 2011; Morales et al., 2017; Burone et al., 2021). It formed during the break-up of the Gondwana supercontinent and the opening of the South Atlantic Ocean (Stoakes et al., 1991; Hinz et al., 1999; Franke et al., 2007; Pérez-Díaz and Eagles, 2014; Conti et al., 2017). Rifting initiated in the Late Jurassic, with movement confined to localised intracontinental accommodation zones before shifting to a central Atlantic rift zone at ~138 Ma (Soto et al., 2011; Pérez-Díaz and Eagles,

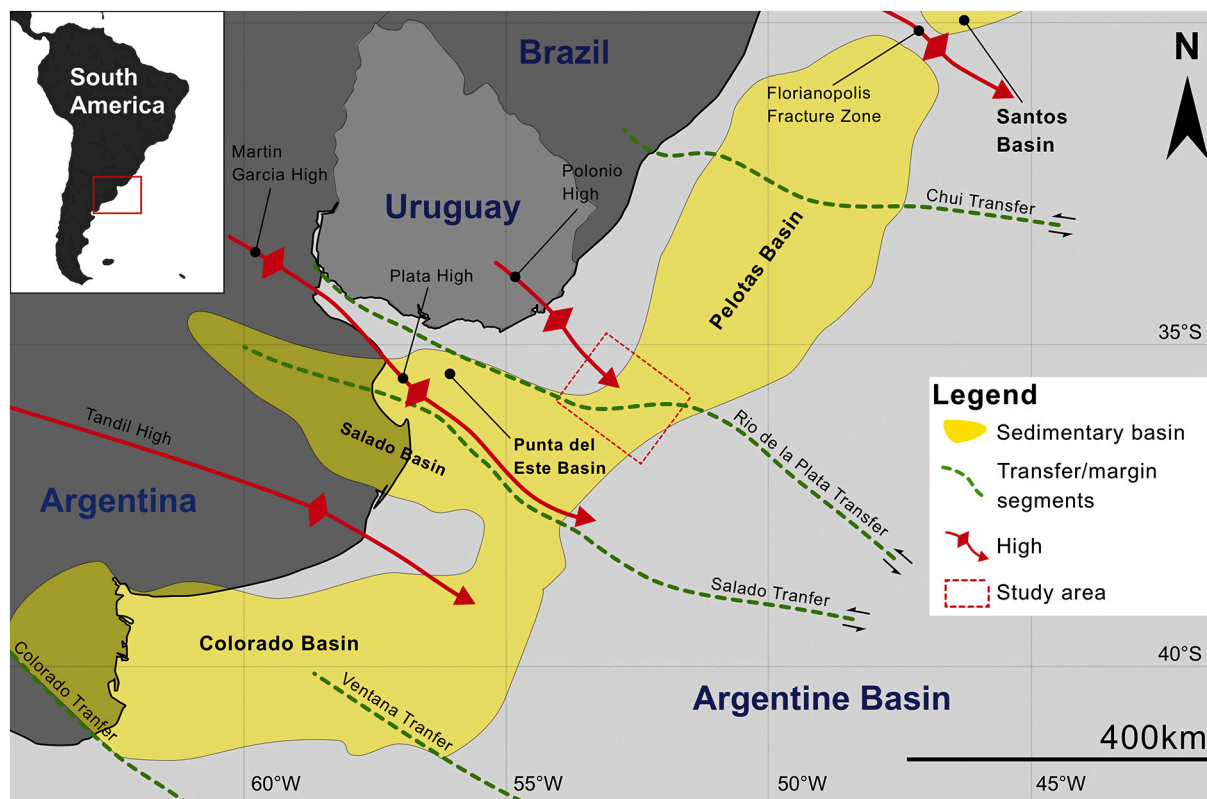


Fig. 1. Structural map of sedimentary basins, geologic highs and fracture zones on the Argentine-Uruguayan Margin (modified from Soto et al., 2011 after Stoakes et al., 1991; Franke et al., 2007). The study area location is indicated with a red box. (For interpretation of the references to colour in this figure legend, the reader is referred to the web version of this article.)

2014; Creaser et al., 2017). Rifting started on the distal margin at ~128 Ma, resulting in thick 60–120 km wide packages of Seaward Dipping Reflectors (SDRs) displayed clearly in seismic records (Franke et al., 2007; Creaser et al., 2017). In the Middle Cretaceous-Paleocene the margin entered a sag/thermal subsidence phase, and became a passive margin in the Eocene-present (Honegger et al., 2018).

Two main basins are found offshore Uruguay (Fig. 1): the Punta del Este Basin (see Stoakes et al., 1991) to the south, and the Pelotas Basin to the north (Soto et al., 2011; Morales et al., 2017; Burone et al., 2021), the latter exhibiting depocentres up to 7 km-thick (Hernández-Molina et al., 2016). The Punta del Este Basin is a funnel-shaped aulacogenetic failed rift basin that formed on continental crust and is related to the Salado and Colorado Basins on the Argentine Margin (Stoakes et al., 1991; Franke et al., 2006; Soto et al., 2011). It has an area of ~50,000 km<sup>2</sup> and is situated to the south of Uruguay, trending northwest-southeast and perpendicular to the margin (Morales et al., 2017). It is separated to the southwest from the Salado Basin (Fig. 1) by the Martín García and Plata Highs and the Salado Transfer System (Stoakes et al., 1991); and from the Pelotas Basin to the northeast by the Polonio High and Río de la Plata Transfer System (Soto et al., 2011; Hernández-Molina et al., 2016; Morales et al., 2017). During the Late Cretaceous, sediment

was predominantly deposited in thick packages of prograding clinoforms, and by the Cenozoic, sedimentation was increasingly influenced by uplift due to Andean tectonics, and eustatic sea level oscillations (Morales, 2013; Hernández-Molina et al., 2016). The Pelotas Basin is a typical NE-SW trending passive margin basin with an area of ~80,000 km<sup>2</sup>. It formed on continental, transitional and oceanic crust and extends from the Polonio High in the south to the Florianópolis Fracture Zone in the north, which separates it from the Santos Basin on the Brazilian Margin (Soto et al., 2011; Hernández-Molina et al., 2016; Morales et al., 2017) (Fig. 1). It exhibits significantly less Late Cretaceous deposits than the Punta del Este Basin, suggesting it was starved of sediment at that time. Yet during the Cenozoic, due to the previously mentioned depocentre shift, thick Paleogene and Neogene deposits are recorded (Hernández-Molina et al., 2016).

The preserved sedimentary record on the margin has four main stages (Soto et al., 2011; Morales, 2013; Hernández-Molina et al., 2016; Creaser et al., 2017; Morales et al., 2017): a) the *prerift stage* involves Proterozoic crystalline basement rocks and Paleozoic continental to marine sediments, b) the *synrift stage* comprises volcanic rocks and continental sediments (Late Jurassic-Neocomian), c) a *transition stage* shows localised intra-basin continental and marine sediments

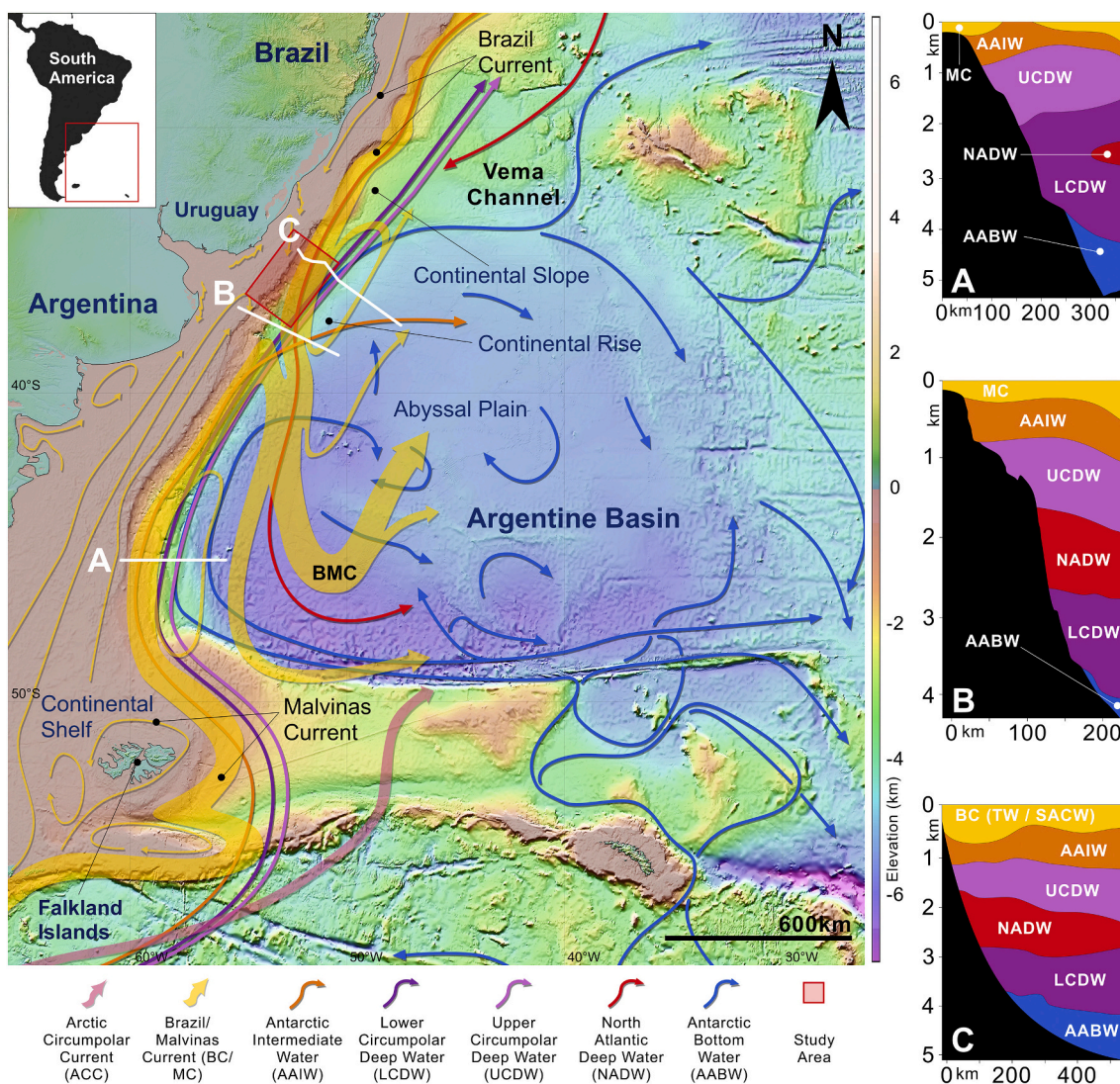


Fig. 2. Present day ocean circulation adapted from Hernández-Molina et al. (2010) after Georgi (1981); Flood and Shor (1988); Arhan et al. (2002a, 2002b). Hydrographic sections offshore South America (A and B) adapted from Hernández-Molina et al. (2010) after Piola and Matano (2001), and (C) from Hernández-Molina et al. (2016). Bathymetric basemap from Tozer et al. (2019).



(Barremian-Aptian), d) and the *post-rift (drift stage)* consists of Late Cretaceous transitional to marine and Cenozoic marine sediments. In the Late Maastrichtian, a single offshore sedimentary province formed as an intra-basin, while external highs were surpassed due to oscillations in the eustatic sea level. These oscillations continued in the Cenozoic and conditioned the sedimentary sequences observed on the margin (Soto et al., 2011).

### 3. Present oceanographic setting

The Argentine/Uruguayan Margin hosts one of the most dynamic ocean regions in the world (Fig. 2), featuring complex surficial, intermediate, deep and bottom water circulations of different water masses flowing in opposite directions relatively close to the seafloor (Piola and Matano, 2001; Arhan et al., 2002b; Hernández-Molina et al., 2009, 2010, 2016; Preu et al., 2013; Thran et al., 2018; Burone et al., 2021). These water masses have different densities due to variations in temperature and salinity and are separated by interfaces in the water column (Fig. 2A, B and C) (Piola and Matano, 2001; Arhan et al., 2002a, 2002b). Changing basin configuration, seafloor topography and the opening/closing of oceanic gateways prior to, and during the Cenozoic, resulted in the complex dynamic thermohaline circulation (THC) and the Atlantic Meridional Overturning Circulation (AMOC) observed today. Pérez-Díaz and Eagles (2017) explain that at ~100 Ma the Falkland Plateau cleared the Cape region of Africa, admitting waters from the Southern Ocean into the South Atlantic, which began the transition towards the present circulation. By ~80 Ma the South Atlantic's ocean basins were deep enough for interconnection at intermediate water depths (1000 m – 2657 m wd), and by 60 Ma the connections between basins allowed for deep water circulation (2657 m – 5597 m wd).

At present day, the surficial circulation (Fig. 2) comprises interactions of the southward flowing Brazil Current (BC), which includes components of Tropical Water (TW) and a highly saline South Atlantic Central Water (SACW), plus the northward flowing Malvinas Current (MC) with primary contributions from the Antarctic Intermediate Water (AAIW) and Upper Circumpolar Deep Water (UCDW). The BC and MC meet to form the Brazil/Malvinas Confluence (BMC) at approximately 38°S offshore Argentina (Stramma and England, 1999; Piola and Matano, 2001; Arhan et al., 2002a, 2002b; Hernández-Molina et al., 2016; Valla et al., 2018). The BMC has a sharp horizontal front in terms of temperature and salinity, and shows intense mesoscale variability leading to amplitude meanders in the mean flow, which causes vertical eddies that propagate away from the front (Gordon and Greengrove, 1986; Piola and Matano, 2001; Combes and Matano, 2014; Hernández-Molina et al., 2016).

Circulation at intermediate depths (Fig. 2) is characterised by the northward flowing AAIW located between about 500 to 1500 m water depth, which originates from surficial waters of the Antarctic circumpolar region, particularly north of Drake's Passage and close to the Falkland Islands (Stramma and England, 1999; Preu et al., 2013).

Deep circulation comprises the northward flowing Circumpolar Deep Water (CDW), which has two separate branches, the UCDW and the Lower Circumpolar Deep Water (LCDW) (Stramma and England, 1999; Arhan et al., 2002a, 2002b; Hernández-Molina et al., 2016); and the North Atlantic Deep Water (NADW), which occupies depths ranging from 1.5 to 2.8 km, between the UCDW and LCDW, it flows southward along the margin before veering eastward (Stramma and England, 1999; Hernández-Molina et al., 2009; Preu et al., 2012; Creaser et al., 2017).

The bottom circulation (>3500 m water depth, Fig. 2) is dominated by the Antarctic Bottom Water (AABW), which becomes partially trapped in the Argentine Basin (Stramma and England, 1999; Hernández-Molina et al., 2009, 2016). The AABW has an upper component consisting of old dense waters derived from the LCDW within the Antarctic Circumpolar Current (ACC), and a lower, denser component that formed in the Weddell Sea offshore Antarctica (Stramma and England, 1999).

The water mass flows up the eastern coast of South America, forming a cyclonic gyre up to 2 km thick in the Argentine Basin (Georgi, 1981; Stramma and England, 1999; Piola and Matano, 2001; Arhan et al., 2002a, 2002b; Hernández-Molina et al., 2016).

## 4. Dataset and methodology

### 4.1. Dataset

The dataset used covers the southern sectors of the Punta del Este and Pelotas Basins and entails (Fig. 3): a) two 3D multichannel seismic (MCS) reflection datasets (BG12 and TO12); b) regional 2D MCS profiles (ANCAP UR11), and c) three wells (Lobo X-1, Gaviotín X-1 and Raya X-1).

#### 4.1.1. Seismic reflection data

##### i) BG12

The BG12 3D survey is a reverse polarity 3D dataset totalling 13,283 km<sup>2</sup> that was acquired by BG/Shell. It lies between 36° – 37°S and 52° – 54°W on the SW Uruguayan Margin, spanning from the continental shelf to the continental rise. The dataset was collected in two phases: a 7420 km<sup>2</sup> area was initially acquired during the first phase between December 2012 and May 2013, this was later merged with a second 6970 km<sup>2</sup> region collected from December 2013 to March 2014. Acquisition parameters are detailed in Table 1. Processing was undertaken by PGS Geophysical and is described in (PGS, 2014). Both areas were initially processed using anisotropic Kirchhoff Pre-Stack Time Migration (PSTM). Later, time-depth conversion was completed using a VTI HyperBeam Velocity Model Building (VMB) and Kirchhoff Pre-Stack Depth Migration within the main processing sequence.

##### ii) TO12

The TO12 survey is a previously unpublished reverse polarity dataset amounting to 7153 km<sup>2</sup> that was acquired by TOTAL S.A. The survey is situated at 35.5°–36.5°S and 51.5°–52.5°W on the central Uruguayan Margin and spans the middle slope to the continental rise; it intersects the Raya X-1 deep water well to the northeast. Processing was undertaken by Schlumberger Geosolutions and TOTAL S.A. between 2013 and 2014, giving an anisotropic Kirchhoff TTI PSDM. This method relies on a four-parameter tomographic velocity model approach to account for the complexity of geological settings like the Uruguayan Margin.

##### iii) ANCAP UR11

The UR11 survey comprises regional reverse polarity 2D MCS profiles totalling 6294 line kms, acquired by Reflect Geophysical. The dataset comprises 58 lines that extend from the continental shelf to the rise between 34.5° and 37.5°S and 51°–55.5°W. Processing was completed by WesternGeco (Schlumberger), the results were a Kirchhoff PSTM and a Kirchhoff PSDM.

#### 4.1.2. Well data

The Lobo X-1 and Gaviotín X-1 wells are located on the continental shelf at 40–50 m water depth (wd) in the Punta del Este Basin (Fig. 3). They were drilled for exploration in the 70's by Chevron. The two wells are intersected by Line UR11–46 from the ANCAP 2D survey detailed above (Table 1). The wells are not representative of the deepest part of the basin, but they do shed light on the stratigraphy (Morales, 2013; Hernández-Molina et al., 2016; Morales et al., 2017). The Raya X-1 deep water well was drilled for exploration by TOTAL S.A. in 2016. It lies on the continental rise in the Pelotas Basin at 3403.7 m wd (Table 2) and is situated within the TO12 survey detailed above. The well targeted an Oligocene basin floor fan and encountered a highly porous 135 m thick



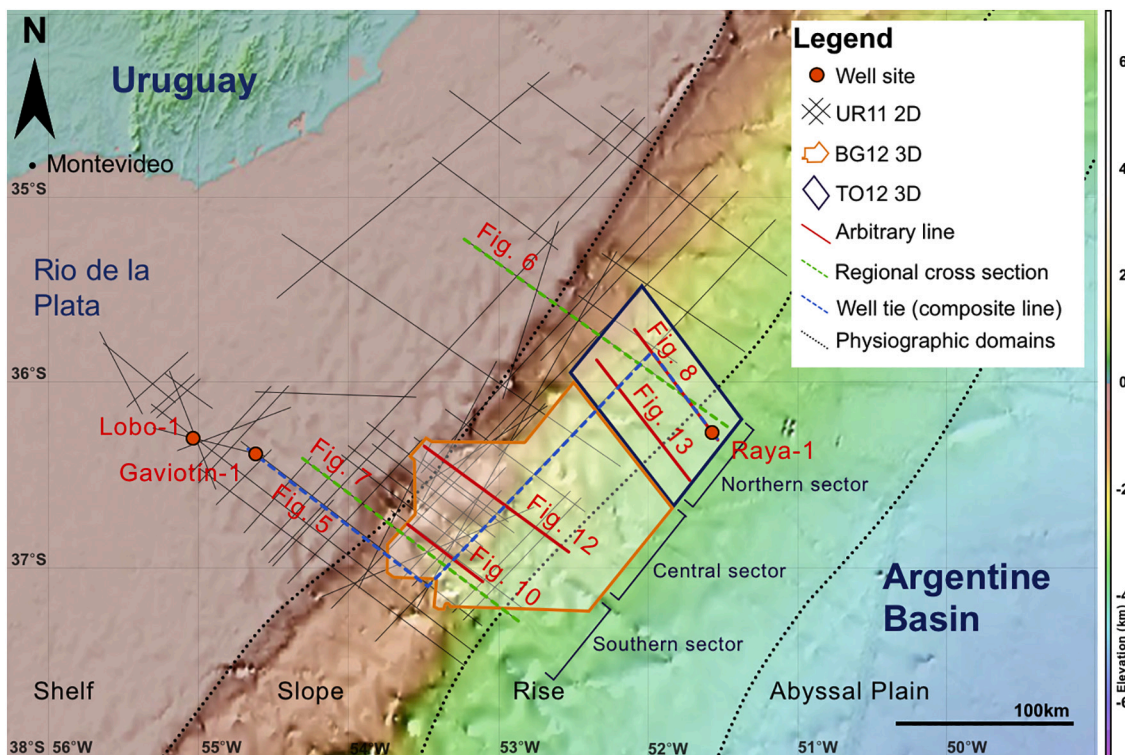


Fig. 3. Map of study area, dataset composite line, regional cross sections and arbitrary line figure locations (1–5). Figures from south to north: BG/Shell crosslines 4500 and 7600 = 1 and 2, Total inlines 4400 and 6200 = 4 and 5. Bathymetry from [Tozer et al. \(2019\)](#).

Table 1  
Seismic survey acquisition parameters (information provided courtesy of ANCAP).

Dataset	Year	Research Vessel (s)	Streamer Length	Streamer Depth	Source Depth	Source Volume	Shot Interval	Group Interval	Sample Rate	Total Area/Lenth
BG12 3D	2012–14	Polarcus Amani	10 × 6000 m	9 m +/- 1	8 m	2 × 4,240 cu. in	25 m	1 12.5 m	2 ms	13,283 km <sup>2</sup>
TO12 3D	2012–14	WG Tasman	12 × 8000 m	9 m +/- 1	6 m	2 × 5,085 cu. in	25 m	\125 m	2 ms	7153 km <sup>2</sup>
“”	“”	WG Regent	10 × 8000 m	“”	“”	“”	“”	“”	“”	“”
UR11 2D	2011	Reflect Aries	8100 m	8 m	6 m	3400 cu.in	25 m/37.5 m	2.5 m	2 ms	6294 km

Table 2  
Wellsite drilling summary (information provided courtesy of ANCAP).

Well	Year	Drilling Rig	Operator	Total depth from origin (m)	Kelly bushing (m)	Longitude	Latitude	Coordiante reference system
Raya X-1	2016	Venturer, Maersk	Total	5856	26	51°33' 57.83"W	36°13'35.15"S	GRS 1980
Gaviotín X-1	1967	Bideford Dolphin	Chevron	3630	25	54°58'08,30"W	36°17'49,60"S	WGS 72
Lobo X-1	1967	Bideford Dolphin	Chevron	2713	25	54°39'52,99"W	36°21'42,94"S	WGS 72

Table 3  
Summary of well formation tops (information for the Gaviotín X-1 and Lobo X-1 wells provided courtesy of ANCAP) ([Alabert et al., 2016](#)).

Raya X-1 Interval	Gaviotín X-1 Interval	TVD (m)	TVD Seismic (m)	Lobo X-1 Interval	TVD (m)	TVD Seismic (m)
Base Pliocene	Upper Miocene	315	290	Upper Miocene	275	250
Late Miocene	Upper Eocene	882	857	Upper Eocene	815	790
Middle Miocene	Lower Eocene	1550	1525	Lower Eocene	1412	1387
Early Miocene	Top Cretaceous	1709	1684	Top Cretaceous	1545	1520
Eocene/Oligocene	Upper Albian	1808	1783			
Late Eocene	Upper Permian	3491	3466			
Middle Eocene	Lower Permian	3560	3535			

sand accumulation, but was ultimately dry (Conti et al., 2017). All wells were tied to the seismic datasets using synthetic seismograms, the Lobo X-1 and Gaviotín X-1 tie has a confidence of  $\sim < 10$  m whilst the Raya X-1 tie has a confidence of  $\sim 1$  m.

A series of formation tops and key chronostratigraphic horizons were obtained for all wells (see Table 3). Well tops for the Gaviotín X-1 and Raya X-1 were used to derive the chronostratigraphic framework of this study, but the depth intervals for the Raya X-1 well were omitted for this manuscript.

#### 4.2. Methodology

Analysis was undertaken at ANCAP's (Administración Nacional de Combustibles, Alcohol y Portland) headquarters in Montevideo, Uruguay, using a HP ENVY laptop and Kingdom Suite™ (IHS) software with a

standard exploration and production (E&P) license. The Kirchhoff PSDM seismic and well datasets were loaded by ANCAP staff. Interpretation of seismic units and facies entailed conventional methods and criteria described in Mitchum et al. (1977) and Catuneanu et al. (2009). 2D lines were used as regional cross-sections and as a chronostratigraphic tie (Fig. 3). Detailed seismic analysis was focused within the 3D datasets, and a series of arbitrary lines served to outline seismic observations. The chronostratigraphy was constrained using a composite seismic reflection profile comprising lines UR11–06 (2D), UR11–39 (2D) and TO12 inline 6200 (3D) to correlate the geophysical data with the Gaviotín X-1, Lobo X-1 and Raya X-1 wells (Fig. 3). In addition, we correlated discontinuities and seismic units with previous authors who have studied the Cretaceous-Paleocene (Creaser et al., 2017), and the Paleogene (Hernández-Molina et al., 2018), following studies which describe much of the sedimentary succession, and from which an age model for the

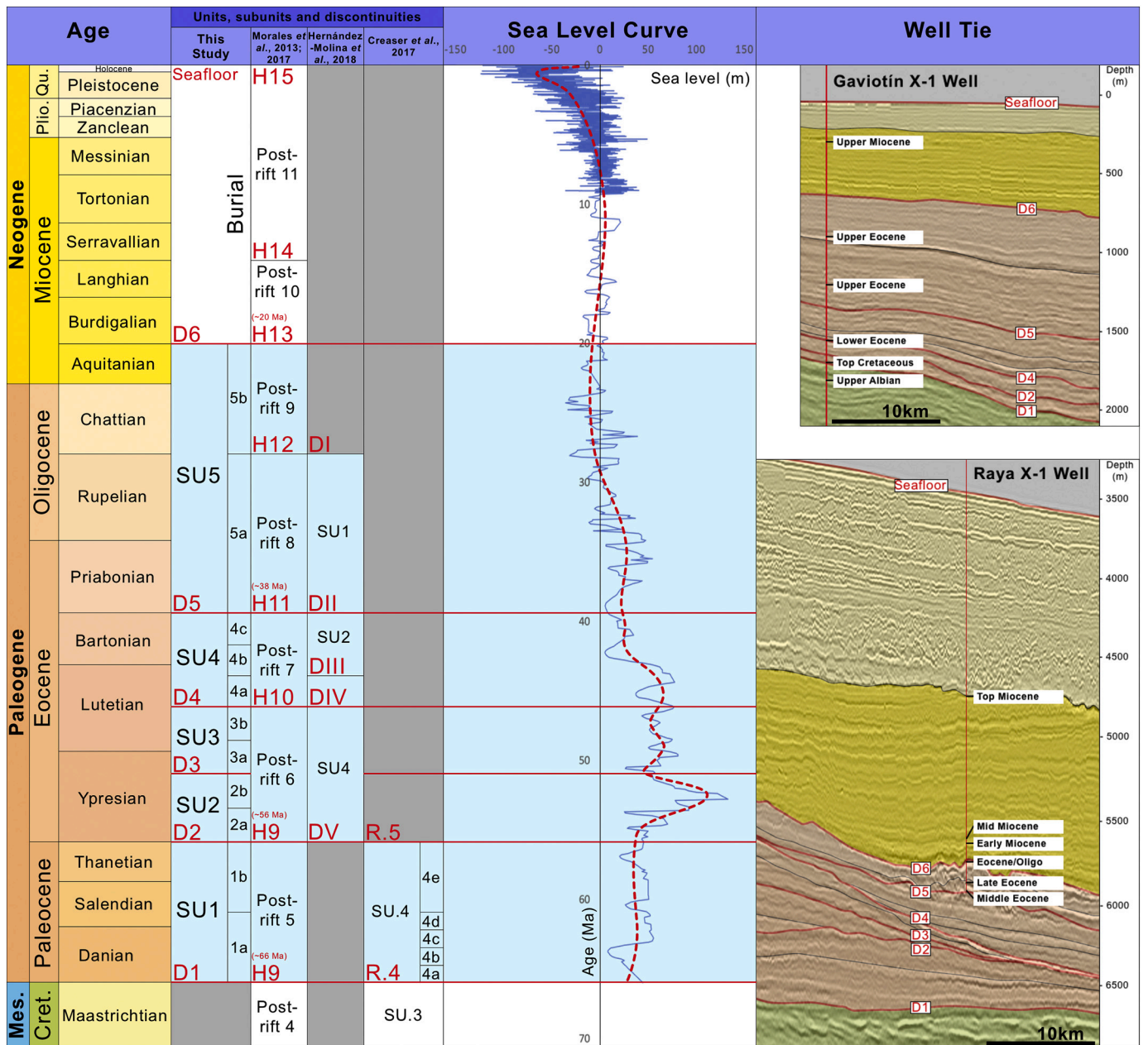


Fig. 4. Chronostratigraphic framework of the interpreted seismic units, subunits and discontinuities based on the Gaviotín X-1 and Raya X-1 wells. In addition to the wells, the discontinuities and seismic units were correlated with those from relevant published literature (Soto et al., 2011; Morales, 2013; Conti et al., 2017; Creaser et al., 2017; Morales et al., 2017; Hernández-Molina et al., 2016, 2018). Sea level curve adapted from Haq et al. (1987) and Miller et al. (2005).



margin has been developed based on biostratigraphy and seismic reflection data (see Morales, 2013; Morales et al., 2017; Conti et al., 2017).

4.2.1. Seismic interpretation of contourite drifts

Bottom current features (contourites) were interpreted at three scales using methods outlined by Faugères et al. (1999), Rebesco and Stow (2001), Stow et al. (2002a), and Nielsen et al. (2008). From large to small, they are: 1) seismic units that trace the overall geometry of a feature and are bound by major regional discontinuities, 2) seismic subunits that are smaller and also bound by discontinuities, and 3) seismic facies that describe the reflection profile and internal configuration. The criteria for contourite drift morphologies and internal configurations are defined by Faugères et al. (1999), Rebesco (2005), and Rebesco et al. (2014).

5. Results

5.1. Chronostratigraphic framework

The studied succession extends from the Uppermost Cretaceous until the Early Miocene (Figs. 4 and 5), it comprises five seismic units (SU1-SU5) (Figs. 4-7) bounded by six regional discontinuities (D1-D6) characterised and summarised in Table 4. The identified key regional discontinuities were mapped across the dataset and correlated where possible with the Gaviotín X-1 and Raya X-1 wells (Fig. 4) and relevant literature (Soto et al., 2011; Morales, 2013; Conti et al., 2017; Creaser et al., 2017; Morales et al., 2017; Hernández-Molina et al., 2016, 2018). D1, D2 and D4 intersect, and were mapped in view of the Gaviotín X-1 well, but were too deep to be penetrated by the Raya X-1 well; therefore, they can be said to approximately correspond to the Top Cretaceous, Paleocene-Lower Eocene and Middle Eocene, respectively. D5 and D6

were identified at both wells and respectively correspond to the Middle Eocene and Early Miocene. The D3 discontinuity is not identified at either Raya X-1 or Gaviotín X-1, proving too deep on the rise and onlapping the slope proximally, it roughly corresponds to the Lower Eocene. The seismic units, when correlated with the literature, point to the following relative ages for the sedimentary succession. SU1 dates to the ~Paleocene (~66 Ma – ~56 Ma) and corresponds with Post-rift 5 in Morales et al. (2017), SU4 in Creaser et al. (2017). SU2 and SU3 extend from the Top Paleocene (~56 Ma) to Middle Eocene (Post-rift 6 in Morales et al., 2017 and SU4 in Hernández-Molina et al., 2018). In turn, SU4 is ~Middle Eocene in age to (Post-rift 7 in Morales et al., 2017 and seismic units SU2 and SU3 in Hernández-Molina et al., 2018), and SU5 extends from the ~Middle Eocene to the Early Miocene at ~20 Ma, subunit 5a correlating with the Post-rift 8 and 5b with the Post-rift 9 of Morales et al. (2017).

5.2. Seismic stratigraphic analysis

Within the study area the Cenozoic sedimentary record is 4274 m thick, whilst the studied succession has a thickness of 3414 m within. Here a very large sedimentary body is identified (Fig. 6), which extends along the middle and lower slope beyond the study area.

5.2.1. Seismic Unit 1 (SU1)

SU1 is the oldest seismic unit, bound at the base by D1 and capped by D2. D1 is an extensive regional discontinuity that appears as a major onlap and downlap surface, it shows evidence of erosion and is characterised by an intermediate to high amplitude reflection (Figs. 6-8). It is cut by major channels (Fig. 5) that can be traced from the middle slope, and extend basinward in a southeast direction. The channels are separated by mounds (C1-C4 in Fig. 5) which extend onto the rise and sometimes show over 1000 m of relief relative to the channels (D1 in

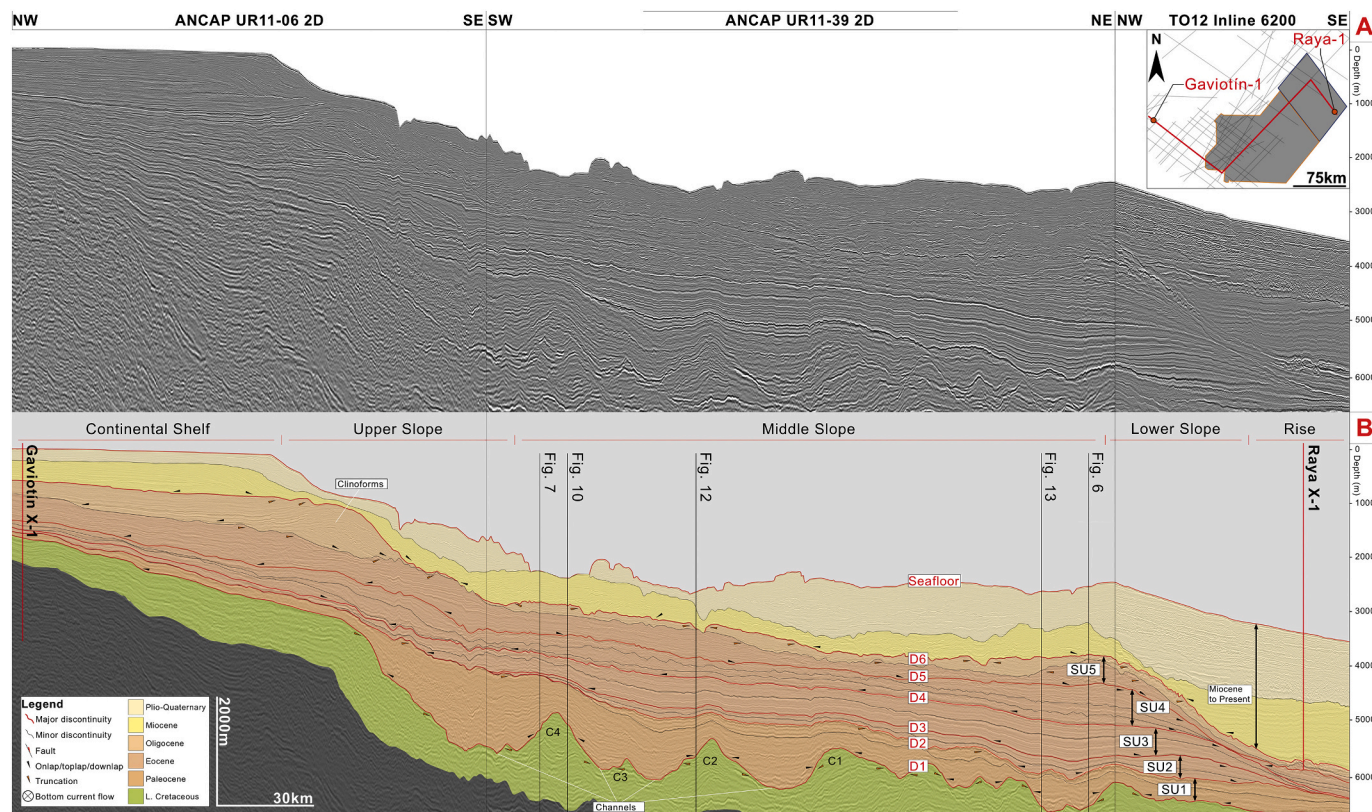


Fig. 5. Uninterpreted (A) and interpreted (B) regional composite line detailing main seismic units and discontinuities of a large contouritic drift body along the studied Uruguayan continental slope, the seismic interpretation key is provided as well as the locations of seismic profiles detailed throughout the results. C1-C4 = channel-drifts crests from Late Cretaceous mixed turbidite-contourite system detailed in Creaser et al. (2017).



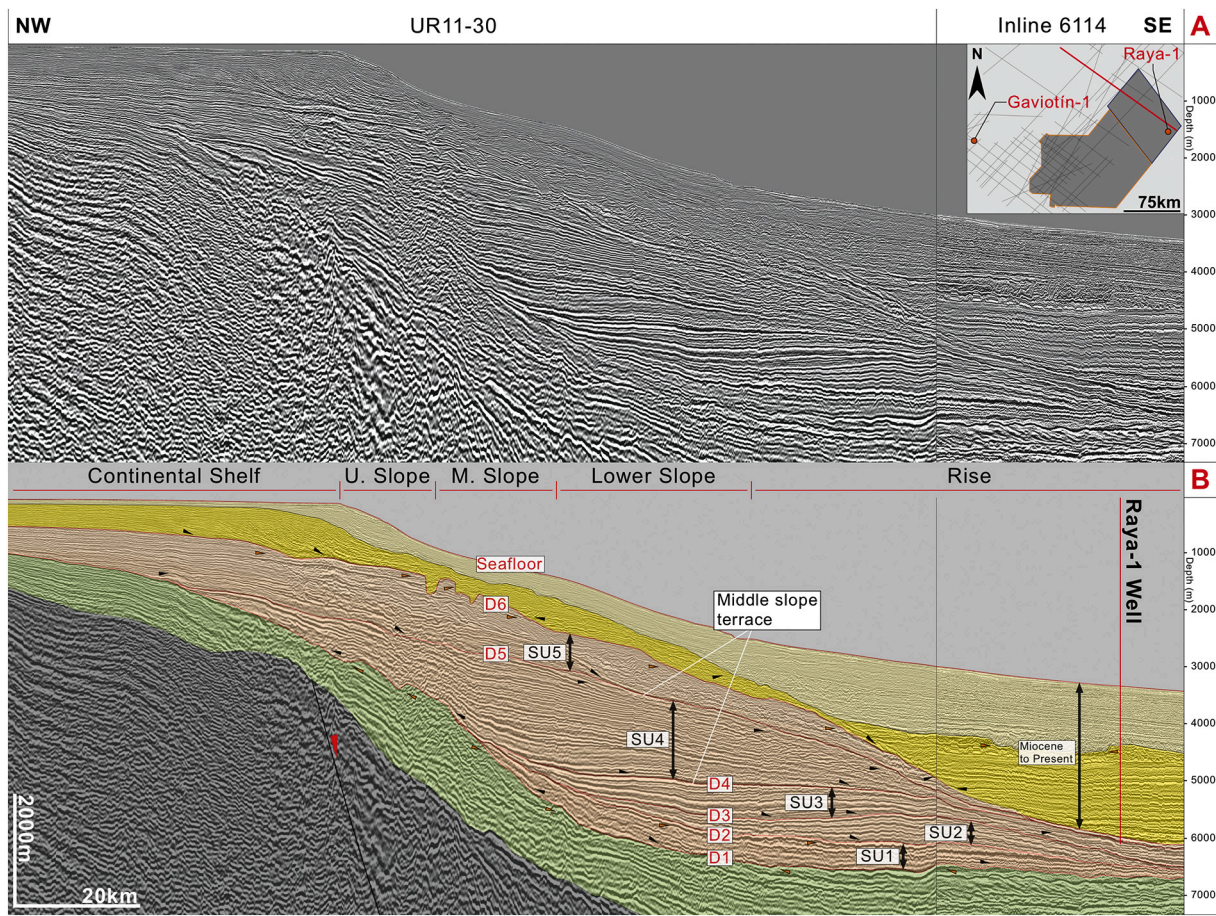


Fig. 6. Uninterpreted (A) and interpreted (B) regional cross-section of a very large contouritic drift body northeast of the studied Uruguayan continental slope, with indication of the main seismic units (SU1 to SU5) and discontinuities (D1-D6) (seismic line courtesy of ANCAP).

Fig. 9). These mounds are particularly evident in the southern sector (Fig. 3).

SU1 is characterised by low to high amplitude stratified parallel and sub-parallel continuous reflections that onlap D1 landwards and basinward. Reflections top lap D2 except where localised truncation is observed along the margin, this is particularly evident to the southwest (see Figs. 10 and 12). The unit has a sheeted configuration, draping across the middle and lower slope; it is deposited predominantly in the southern sector, where it has a maximum sedimentary thickness of 1642 m (Fig. 11). Towards the northern sector the unit thins, but increases in amplitude. Normal faults are observed within SU1 in the southern and central sectors (see Figs. 10 and 12), and in the northern sector above bathymetric highs and on the rise (see Figs. 8 and 13).

The unit comprises two subunits (1a and 1b), as summarised in Table 5. Subunit 1a is deposited in northwest-southeast oriented depocenters and is confined by the bathymetric highs described in the D1 surface. It has a thickness of 1171 m on the middle slope with a mean thickness of ~800 m. In turn, 1b has a maximum thickness of 1259 m and a mean thickness of ~750 m in its primary depocenter; it is less confined, forming a lateral sheet.

### 5.2.2. Seismic Unit 2 (SU2)

SU2 is bound basally by D2 and capped by D3. D2 is a local discontinuity that shows evidence of erosion and is characterised by a high amplitude reflection, it can be observed from the shelf to rise in the southern sector, and terminates against the middle slope further northwards (Figs. 6-8). Some morphological elements identified in D1, inherited through SU1, can be seen in the D2 discontinuity surface (Fig. 9).

The unit exhibits low to mid amplitude stratified parallel and sub-parallel reflections in the southern sector, that increase to high amplitude divergent and wavy reflections in the northern sector. Reflections onlap D2 proximally on the middle slope and southwards where the unit thins, gentle downlapping is observed basinward on the rise. With respect to D3, reflections top lap landwards and basinward, localised truncation is observed in distal domains (Fig. 7). Although SU2 is situated mostly on the lower slope, it has a sheeted configuration in the southwest sector, where it exhibits a thickness of <250 m. It becomes increasingly mounded to the northeast, showing a maximum sedimentary thickness of 673 m (Fig. 11). Landward of the mound an along-slope channel (moat) is observed, it is wide and deep with some deposition in the northern sector and become increasingly narrow and shows evidence of erosion in the southern sector, the moat is associated with 'high amplitude reflections' (HARs) (see Figs. 8 and 10).

SU2 comprises subunits 2a and 2b (Table 5), separated by a high amplitude intra-drift discontinuity. 2a marks a depocenter shift from the southern to the northern sector. It has a maximum thickness of 428 m and a mean thickness of ~275 m within 8 northwest-southeast trending depocenters associated with bathymetric lows identified in the D2 surface (Figs. 9 and 11). In turn, 2b has a less confined depocenter that extends along the middle slope, it has a maximum thickness of 459 m and a mean thickness of ~300 m.

### 5.2.3. Seismic Unit 3 (SU3)

SU3 is bound by D3 at the base and capped by D4. D3 is a prominent intra-drift discontinuity characterised by an intermediate to high amplitude reflection, it locally truncates SU2 and terminates against the slope (Fig. 10).



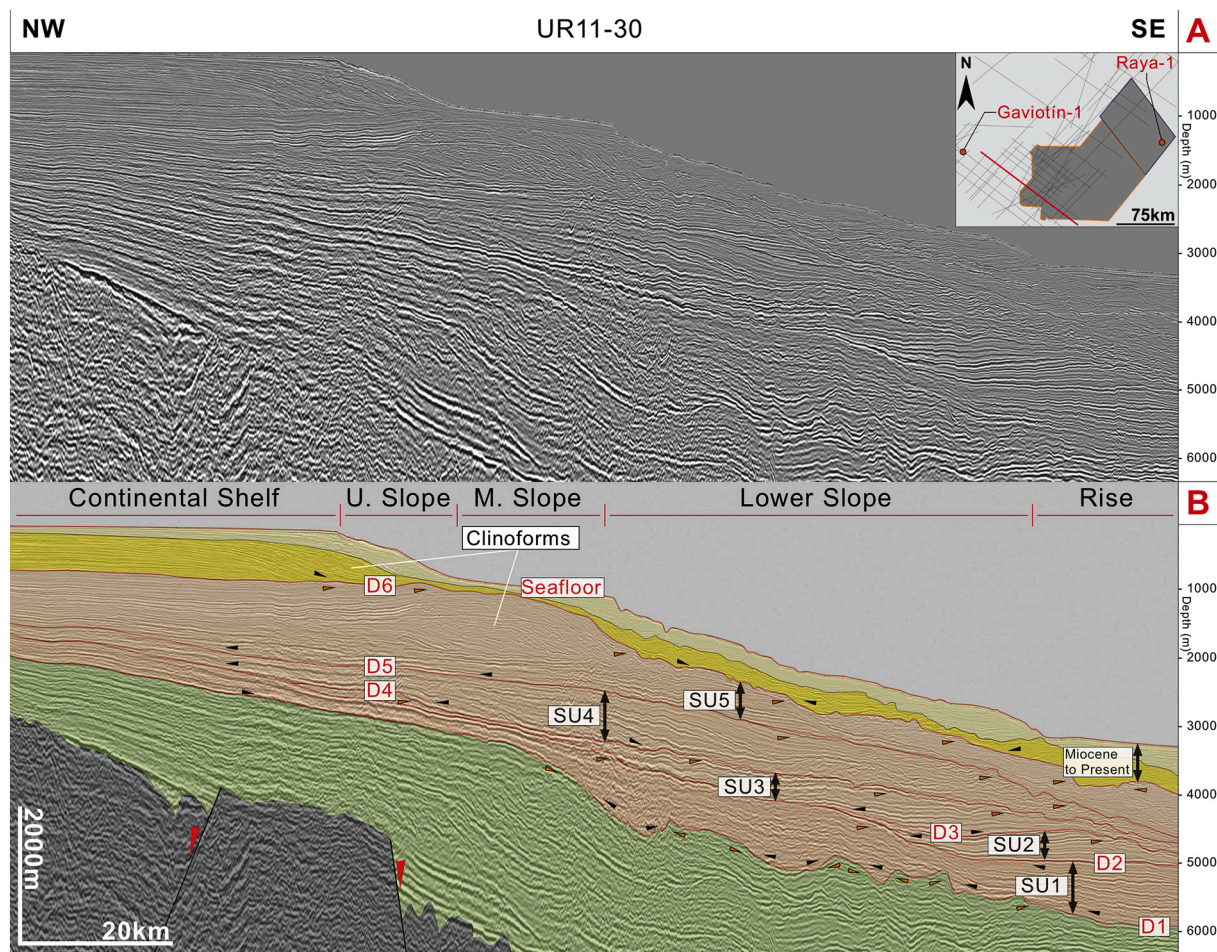


Fig. 7. Uninterpreted (A) and interpreted (B) regional cross section of a large contouritic drift body southwest of the studied Uruguayan continental slope, with indication of the main seismic units (SU1 to SU5) and discontinuities (D1 to D6) (seismic line courtesy of ANCAP).

Internally SU3 exhibits low to very high amplitude parallel, sub-parallel, divergent, wavy and transparent reflections (Figs. 8 and 12). Onlapping is observed against D3 on the middle slope and within the moat in the northeast sector (Fig. 8), whereas downlapping is observed basinward on the lower slope and rise. The unit toplaps D4 basinward in the north and becomes increasingly truncated by the discontinuity to the south across the middle slope, most clearly in the central sector of the dataset (Figs. 10 and 12). SU3 has a sheeted configuration and is situated on the middle slope, which becomes a more distinct domain (D4 in Fig. 9), being thickest in the northeast sector, up to 702 m (Fig. 11). HARs are observed more landwards on the middle slope associated with the bounding discontinuities and throughout SU3 (Fig. 12).

The unit comprises two subunits (3a and 3b) summarised in Table 5. The primary depocenter of 3a is situated within the moat and extends along the middle slope, reaching a maximum sedimentary thickness of 426 m, with a mean thickness of 270 m. The depocenter of 3b lies in the south to central sector, on the middle slope, having a maximum thickness of 459 m and a mean thickness of 290 m.

#### 5.2.4. Seismic Unit 4 (SU4)

SU4 is bound at the base by D4 and capped by D5. D4 is a prominent regional discontinuity characterised by an intermediate amplitude reflection in the northern sector that increases further south where the discontinuity truncates SU3 (Figs. 10 and 12). D4 extends onto the shelf in the southern sector of the dataset and terminates against the upper slope in the northeast sector.

SU4 is characterised by low amplitude sub-parallel to divergent reflections on the shelf and upper slope, mid to very high amplitude

parallel, sub-parallel and wavy reflections across the middle slope, and low to mid amplitude parallel, sub-parallel, transparent and chaotic reflections on the lower slope and rise. Reflections downlap D4 landward and seaward, and toplap D5 basinward. The unit is locally truncated by D5 in the southern sector and pinches out on the lower slope (Fig. 10). SU4 has a lenticular mounded configuration in the southwest sector that becomes more sheeted seaward and in the northern sector (Figs. 8 and 13), while the middle slope domain broadens and extends northwards (D5 in Fig. 9). The unit thickens towards the northern sector, where it reaches 1446 m, and shows HARs at its base landward on the middle slope (Figs. 8 and 11).


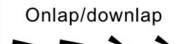

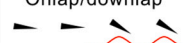
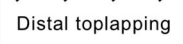

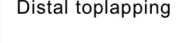




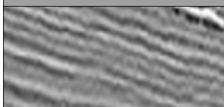

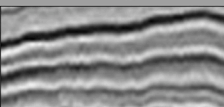
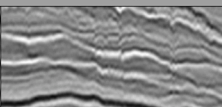
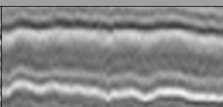

SU4 comprises 3 subunits (4a, 4b and 4c), as summarised in Table 5. The primary depocenter of 4a is situated in the central and northern sectors, where the subunit has a maximum thickness of 614 m. In 4b the depocenter is bifurcated with two strands extending along-slope and ranging in width from ~10 km to ~38 km; they unify further north, showing a maximum thickness of 590 m and a mean thickness of 370 m. A bifurcated depocenter is also observed in 4c, with a maximum thickness of 600 m, and strands of similar width (~20 km).

#### 5.2.5. Seismic Unit 5 (SU5)

SU5 is bound by D5 at the base and capped by D6. The D5 discontinuity shows evidence of erosion and is characterised by an intermediate to high amplitude reflection, it is laterally continuous and can be traced from the shelf to the rise (Fig. 7).

Internally low to high amplitude parallel, sub-parallel, divergent, transparent and chaotic reflections are observed. The reflections onlap D5 in a landward direction and gently downlap basinward, they also

**Table 4**  
Seismic Units.

Seismic Unit	Age	Discontinuity and Surface	Reflection Termination	Internal Configuration and Shape					
				Shelf	Slope	Rise			
<b>SU5</b>	Late Eocene - Early Miocene	<b>D6</b> Regional high amplitude negative, erosive discontinuity that is continuous on shelf	Truncation 	Low to high amplitude parallel and sub parallel reflections in a sheet	Low to mid amplitude parallel, sub parallel, divergent, wavy and transparent reflections in a locally eroded sheet/lenticular mound	Low to high amplitude parallel, sub parallel, transparent and chaotic reflections in a sheet to irregular mound			
		Onlap/downlap 							
<b>SU4</b>	Middle Eocene	<b>D5</b> Regional negative and positive reflection with localised erosion	Toplap/truncation 	Low to mid amplitude parallel reflections in a sheet	Low to high amplitude sub parallel, divergent and wavy reflections in lenticular mound to aggradational sheet	Low to high amplitude parallel, sub parallel, transparent and chaotic reflections in a sheet to irregular mound			
		Onlap/downlap 							
<b>SU3</b>	Lower Eocene	<b>D4</b> Regional continuous negative reflection with local erosion on the middle slope	Distal toplapping 	N/A	Low to high amplitude sub parallel, transparent and wavy reflections in an aggradational sheet	Low to mid amplitude parallel and sub parallel reflections in a sheet			
		Onlap/downlap 							
<b>SU2</b>	Lower Eocene	<b>D3</b> Extensive positive reflection on the middle slope to rise with local erosion	Distal toplapping 	N/A	Low to high amplitude parallel, sub parallel, divergent and wavy reflections in an aggradational sheet to mound	Low to mid amplitude parallel, sub parallel and wavy reflections in a sheet			
		Onlap/downlap 							
<b>SU1</b>	Paleocene	<b>D2</b> Laterally continuous regional positive reflection with localised erosion	Toplap/truncation 	Low to high amplitude parallel and sub parallel reflections in a sheet	Low to high amplitude parallel, sub parallel, divergent and transparent reflections in a locally eroded sheeted drape	Low to high amplitude parallel and sub parallel reflections in a locally eroded sheeted drape			
		Onlap/downlap 							
<b>Pre-drift sequence</b>	Late Cretaceous	<b>D1</b> Highly erosive positive and negative regional reflection	Toplap/truncation 	Low to high amplitude parallel and sub parallel reflections in a basinward thickening sheet	Low to high amplitude parallel, sub parallel, divergent, wavy and transparent reflections in margin perpendicular mounds and channels	Low to high amplitude parallel, sub parallel, divergent, wavy and transparent reflections in margin perpendicular mounds and channels			
				<b>Parallel</b>	<b>Sub parallel</b>	<b>Divergent</b>	<b>Wavy</b>	<b>Transparent</b>	<b>Chaotic</b>
									

toplap D6 basinward and are locally truncated across the upper and middle slope. Across the continental shelf, reflections are stratified; in contrast the upper slope is initially characterised by divergent reflections in a lenticular mound above which, basinward progradation is observed, the unit reaches a maximum thickness of 1309 m in the southern sector (Fig. 11). Across the middle slope, the unit is sheeted and initially exhibits sub-parallel continuous intermediate to high amplitude reflections that become more discontinuous, and sometimes indistinct towards its top. The unit has a mean thickness of ~500 m except in the central sector, where it thins to <~300 m (Fig. 12). SU5 extends on to the lower slope (Fig. 13), showing a mean thickness of <~600 m in lenticular mounds characterised by stratified intermediate amplitude reflections that onlap D5 landward and top lap D6 basinward. The unit thins landwards across the middle slope, where increased evidence of erosion is observed (SU5 in Fig. 11). Across the rise, the unit appears as a thin sheet of low to intermediate amplitude parallel and sub-parallel reflections, some localised chaotic reflections being observed in the northern sector (Fig. 13). In SU5 the middle slope broadens, extending further to the northeast (Fig. 9).

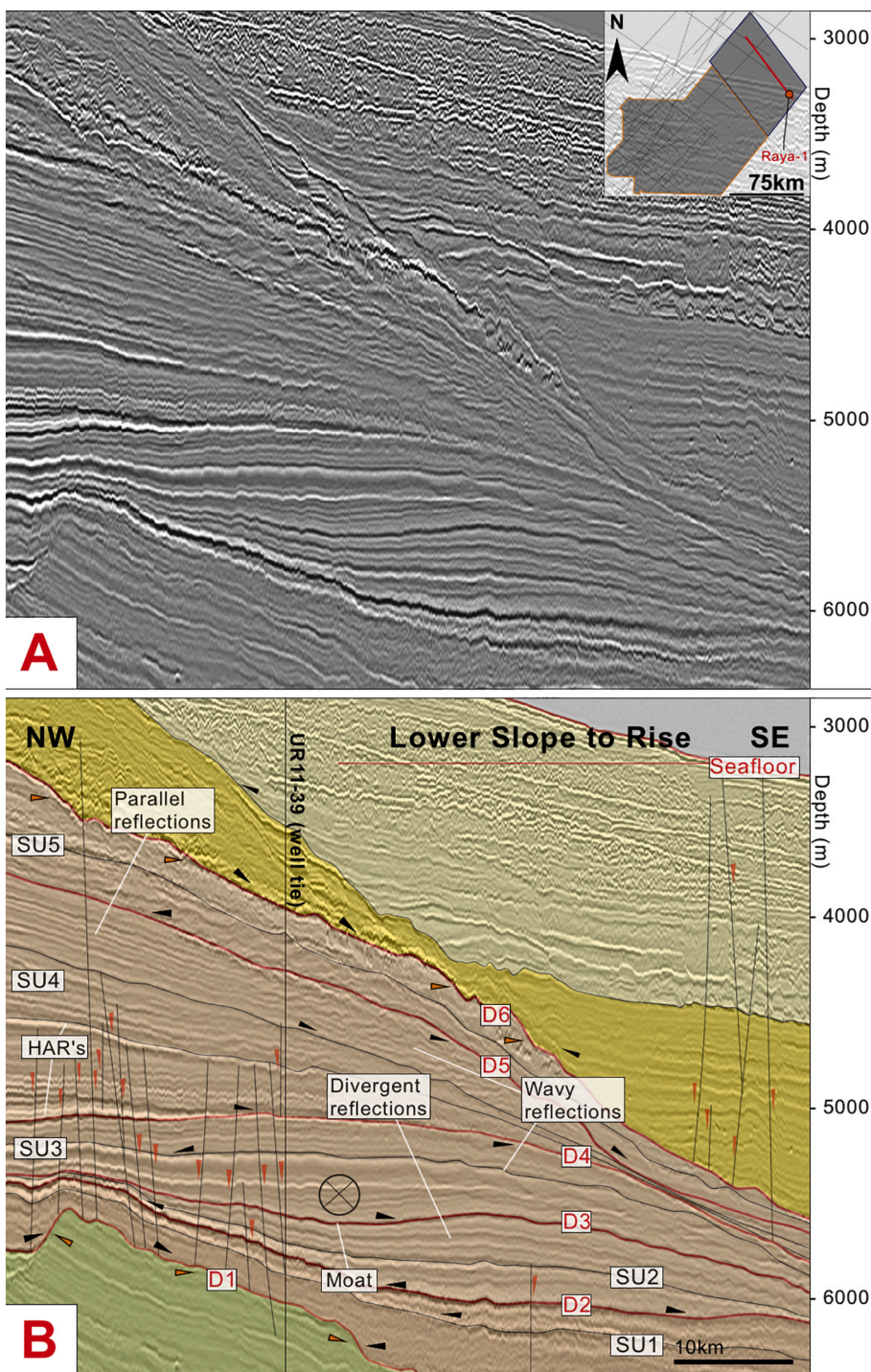
SU5 has two subunits (5a and 5b) that are summarised in Table 5: 5a is observed predominantly in the northern and southern sectors across the upper, middle and lower slope and has a maximum thickness of 473 m; 5b is observed along-slope, with the primary depocenter on the upper slope where it has a maximum thickness of 697 m (see Figs. 7 and 11).

#### 5.2.6. Miocene to present

The Miocene to present day sedimentary record is not analysed in detail in this work, but we offer some general considerations. Its basal boundary is D6 (Fig. 9) and it extends to the present-day seafloor. D6 is a prominent regional discontinuity that shows evidence of significant erosion (see Fig. 12), it is characterised by a low amplitude reflection on the shelf and to the south on the rise, to a high amplitude one across the slope. In the northern sector on the rise D6 coincides with chaotic reflections.

Internally on the shelf, this sedimentary record features relatively continuous parallel and sub-parallel reflections that downlap D6 and top lap at the seafloor landwards. On the slope, high amplitude parallel and sub-parallel discontinuous reflections onlap proximally, though





**Fig. 8.** 3D inline 6200 detailing key seismic observations in the northeast sector. The main seismic units (SU1 to SU5) and discontinuities (D1 to D6) are shown (courtesy of ANCAP. Original seismic data acquired by TOTAL). A predominantly aggradational stacking pattern is observed in SU1 to SU3, while in SU4 a subtle progradation is seen at the base, and a more aggradational stacking pattern is observed towards the top of the unit and in SU5. From SU2 to SU4 the units stack landward. This is particularly evident between SU3 and SU4. A key characteristic of the northern sector is the subtle mounded configuration of SU2, which shows divergent and wavy reflections, and a concave channel extending along-slope. Normal faults cut the succession over a bathymetric high described from D1.

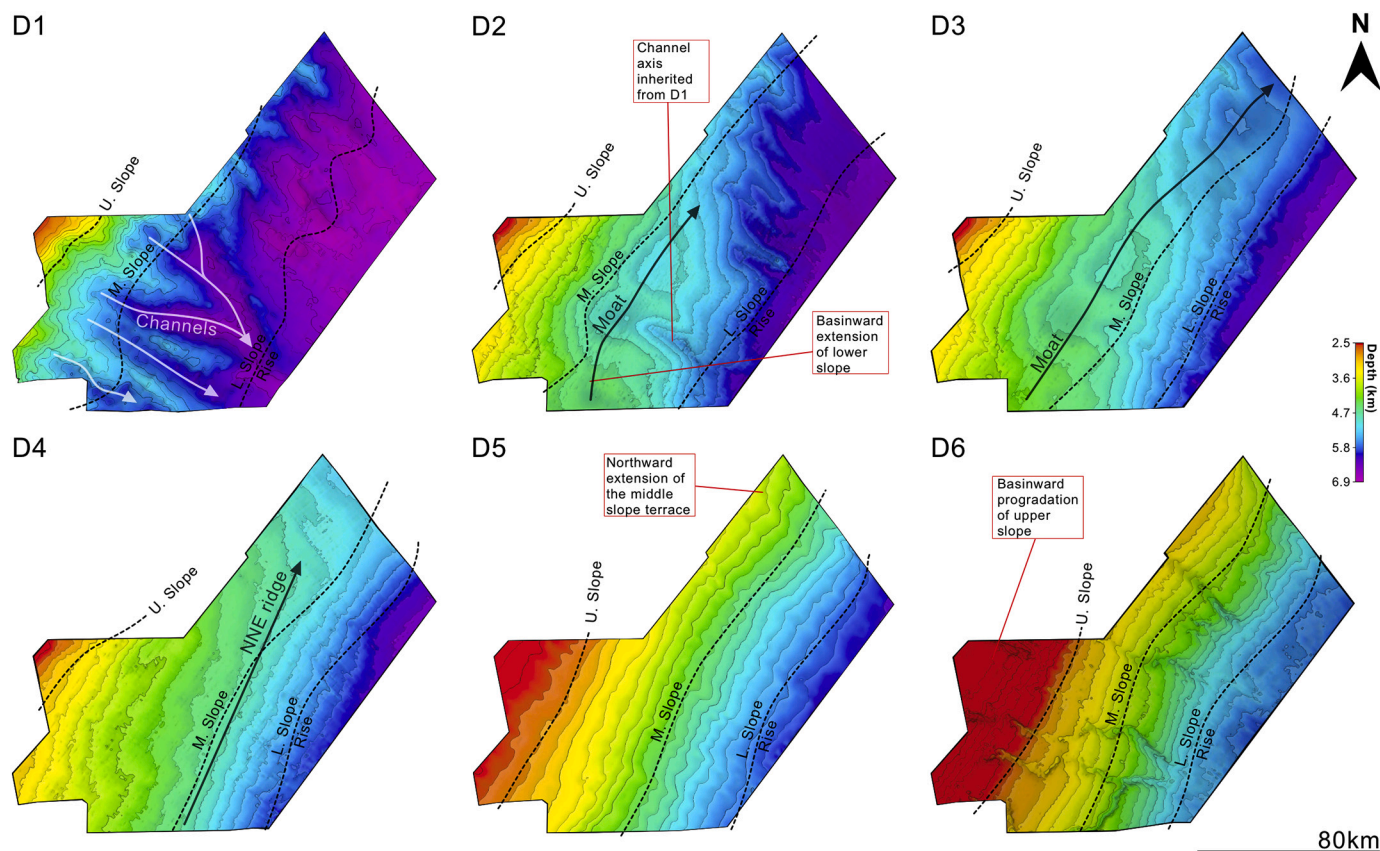
later the reflections decrease in amplitude —sometimes becoming transparent but increasing in lateral continuity. Toplapping is observed against the seafloor basinward and the unit is frequently truncated (Figs. 7, 12 and 13). Across the rise reflections at the base of the unit are low to high amplitude sub-parallel to slightly divergent basinward, and overlap the continental slope landwards. Younger deposits exhibit parallel, sub-parallel, transparent and chaotic discontinuous reflections that overlap the slope, with shallow truncation observed at the seafloor.

Above D6, the primary depocenter on the margin shifts from the middle slope, where the studied sedimentary body developed, to the rise (Fig. 13). Across the shelf the unit has a thickness of ~850 m and on the slope it increases up to ~1050 m. In the primary depocenter thicknesses

reach 1525 m (Fig. 11). Extensive normal faults are observed throughout the unit in this domain (Fig. 13).

### 5.3. Main along-slope and down-slope features

A number of main depositional and erosive features were identified at the seismic scale within the studied seismic units of the Paleogene succession along the Uruguayan Margin.



**Fig. 9.** Key surfaces for the main regional discontinuities identified (D1 to D6), where the main along- or across-slope features are included (see the text for further explanations), surfaces have a Z factor of 10 and show shaded relief.

### 5.3.1. Along-slope (bottom current) depositional features: Drifts and sedimentary waves

#### i) Contouritic drift

The studied succession corresponds to a large contouritic plastered drift, based on its large-scale seismic characteristics and following Faugères et al. (1999). It extends across the slope of the Uruguayan Margin and beyond the extent of the dataset, its primary depocenter lying on the middle slope. The drift initiated in SU1 and developed through SU5. In the northern sector it has a cumulative thickness of 2900 m and an across slope width of 160 km, while in the southern sector it has a maximum thickness of ~3414 m and a width of 150 km (Figs. 6 and 7).

#### ii) Sedimentary waves

Wavy reflections were identified at the transition from the middle to lower slope, they are exhibited within SU2 and SU3 in the central and northern sectors, and in subunits 4b and 4c across all sectors (Figs. 10 and 13). They have wavelengths up to 4.5 km, wave heights up to 120 m, a lateral length of ~1–3 km and indicate a westward upslope migration. Reflections in the sedimentary waves vary in amplitude but are generally low to intermediate.

### 5.3.2. Along-slope (bottom current) erosional features: Contourite moat

A moat identified in SU2 is subtle and partially truncates SU1 to the southwest, then evolves along-slope towards the northern sector, showing up to 120 m of aggradation (see Figs. 8–10 and 13). It has a width that ranges from ~10 km in the southern sector up to ~32 km in the northern sector; its depth is from ~30 m up to 80 m (S–N). Internally

the moat is associated with HARs which are observed clearly in the southern sector (Fig. 10).

### 5.3.3. Along-slope mixed (depositional and erosional) features: Contourite terraces

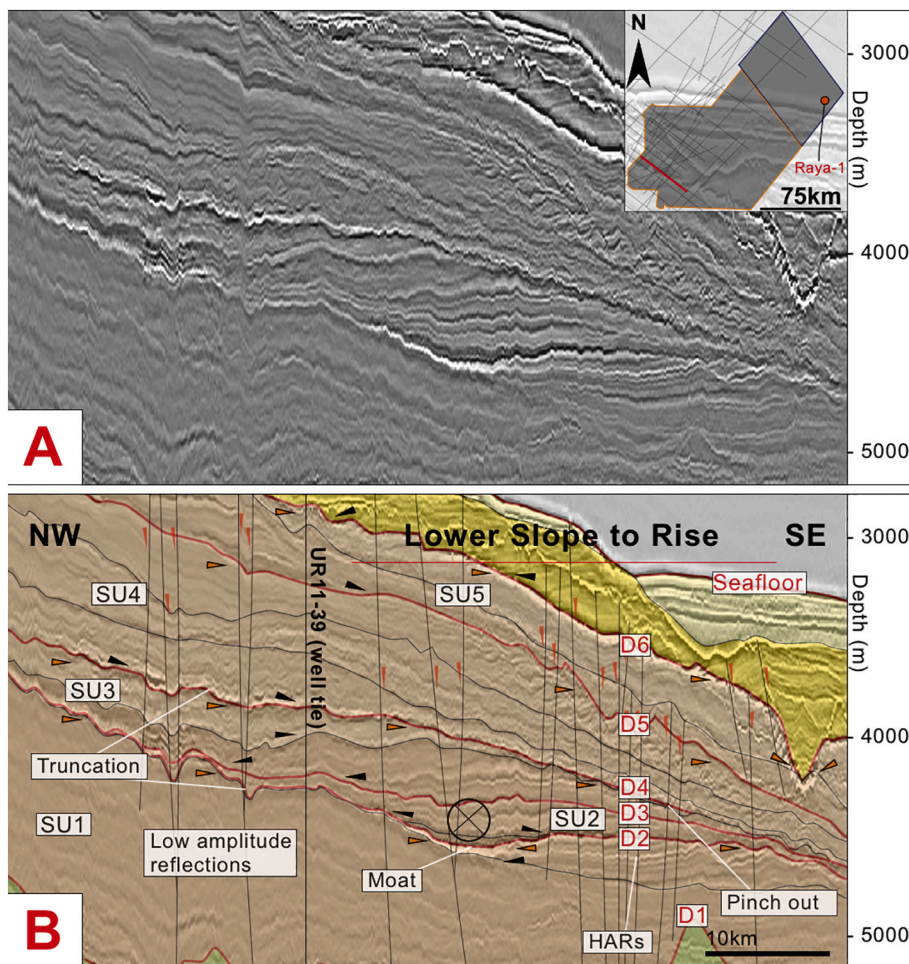
Terraces are located across the middle slope at the top and landward parts of most of the seismic units of the large plastered drift (Figs. 6, 12 and 13). They trend north-northeast and are associated with the bounding discontinuities D2–D6. In D2 the terrace dips shallowly landwards into the moat with a gradient of  $0.36^\circ$  (D2 in Fig. 13), except across bathymetric highs (see Fig. 12), where a flat or slightly seaward dipping surface is observed which shows increased evidence of erosion. In D3–D6 the terrace dips seaward with a mean gradient of  $0.98^\circ$ ; it is separated from the lower slope by a north-northeast trending ridge (see D4 to D6 in Fig. 9). Local wavy reflections are often associated with the basinward part of the terraces and widespread HARs are observed across them (Figs. 12 and 13).

### 5.3.4. Down-slope (gravitational) features

Deposits with clinofolds are identified on the upper continental slope in its southern sector (see Figs. 5 and 7). A thick package of clinofolds prograded approximately 33 km (D6 in Fig. 9) south-eastward into the survey in SU5. They have a maximum thickness of ~800 m and can be viewed in Fig. 7. Clinofolds were further observed in the Miocene to present sedimentary record.

Chaotic reflections seen in SU4 and SU5 on the rise in the northeast sector (see Fig. 13) represent mass transport deposits (MTDs) at the base of slope. Down-slope submarine canyons were identified in the D6 discontinuity, which truncates SU5 (Fig. 11). They are linked to a change in the depositional system during the Miocene to present (see Figs. 9 and 10).





**Fig. 10.** Crossline 4500 detailing key seismic observations in the West of the southern sector. The main seismic units (SU1 to SU5) and discontinuities (D1 to D6) are shown (courtesy of ANCAP. Original seismic data acquired by BG/Shell). SU1-SU3 show an aggradational stacking pattern which becomes progradational in SU4, in SU5 the stacking pattern is more aggradational. The units step landward between SU2 and SU4, while in SU5 aggradation is focused in proximal and distal domains. SU1 is thicker in the southern sector and the onset of aggradation is clearly observed in high amplitude reflections at the top of the unit; SU2 and SU3 are thinner in the southern sector. D2 shows localised erosion in a small channel that is the southern extent of the wider channel observed in the northern sector. D4 is highly erosive further South, clearly truncating SU3 on the middle slope. Normal faults are observed throughout all units, showing minor displacements.

## 6. Discussion

### 6.1. Sedimentary interpretation and stacking pattern

#### 6.1.1. Interpretation

The studied succession corresponds to a large plastered drift along the Uruguayan margin based on seismic facies and along-slope distribution as some authors have proposed in other continental margins (McCave and Tucholke, 1986; Faugères et al., 1999; Miramontes et al., 2019; Rodrigues et al., 2020). It is bounded by the prominent and erosive basal and top discontinuities D1 and D5, and has its primary depocenter across the middle slope (Figs. 5 and 11). The drift is identified by a distinct convex geometry in the northern sector where sediment is focused towards the centre, and a more elongated geometry in the southern sector (see Figs. 7 and 8). Reflections range from more typical transparent low amplitudes (see Faugères et al., 1999) to very high amplitudes, and the seismic units have a broad sheeted to slightly mounded configuration that changes both laterally and vertically. The proximal part of the drift is associated with erosive along-slope features and displays an evolution from a moat or an erosive terrace across bathymetric highs in SU2, to a broad depositional terrace across the middle slope that is maintained until SU5; both the moat and terrace, which are associated with increased bottom current activity (Rebesco et al., 2014) exhibit HARs whilst sedimentary waves are observed more seawards throughout the drift succession, suggesting that these secondary features are linked to bottom current activity. Similar general characteristics are described for other large plastered drifts in continental margins (Rebesco et al., 2014; Hernández-Molina et al., 2018; Miramontes et al., 2019; Thiéblemont et al., 2019; Rodrigues et al.,

2020).

#### 6.1.2. Sedimentary stacking pattern

Even though the plastered drift is a basin scale feature, the distinctive lateral and vertical changes within the sedimentary stacking pattern, described below, explain major changes in its overall geometry along-slope (Figs. 6 and 7). One important distinction entails lateral shifts between the seismic units. Between SU1 and SU2, the primary depocenter shifts along-slope from the southern to the northern sector. Then, between SU2 and SU4, a retrograde stacking pattern is observed. In SU5 the depocenter becomes more distal again, as with SU1 and SU2 (Fig. 11).

SU1 has an aggradational stacking pattern, as mentioned, it is preferentially deposited in NW-SE oriented bathymetric lows, these lows represent downslope channels and are separated by channel-drifts (C1-C4 in Fig. 5) which together form a mixed turbidite-contourite system described by Creaser et al. (2017). Generally speaking, SU1 is a wedge that is thickest in the southern sector, it thins along-slope by 100's of meters, and narrows to the point of pinching out proximally in the northern sector (Fig. 11). Within subunit 1b aggradation becomes localised on the lower slope (~40 km basinward of subunit 1a), and is associated with HARs (Figs. 9, 12).

SU2 is also aggradational and lies near subunit 1b, on the lower slope. Its primary depocenter is in the northern sector (~70 km northward of SU1), where it infills more subtle NW-SE oriented bathymetric lows, and forms a subtle mound (subunit 2b in Figs. 8 and 13). Overall the unit is wedge-shaped; it thins towards the southern sector in conjunction with erosion. The unit likewise thins across the middle slope where the bottom current core is focused; yet in the northern sector this



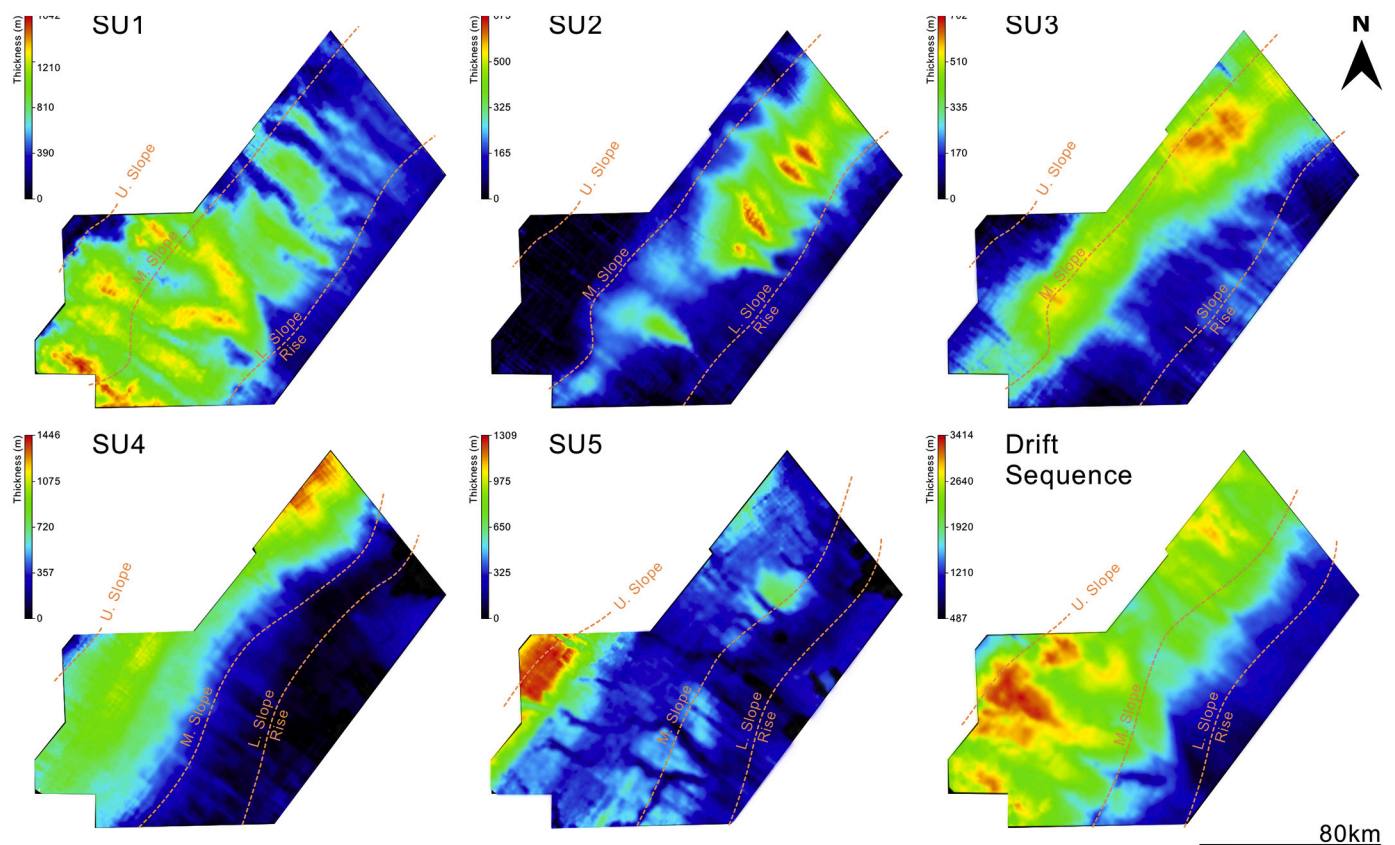


Fig. 11. Seismic unit thickness maps, where the main along- or across-slope depocenters are shown (see the text for further explanations).

creates the landward-dipping terrace adjacent to the moat and mound (Figs. 8, 10 and 13).

In SU3 the stacking pattern is aggradational. The unit is localised on the middle slope (~28.5 km landward of SU2 in the northern sector, 22.5 km in the southern sector), thus establishing the middle slope terrace (Figs. 6 and 13). Subunit 3a infills the moat of SU2 and forms a wedge due to increased accommodation space in the northern sector (Figs. 10, 11 and 13). Subunit 3b is more evenly distributed across the middle slope, with higher levels of aggradation seen for the central and southern sectors.

In SU4 the stacking pattern changes, towards the southern sector obliquely basinward progradational reflections are observed (Fig. 7), whilst further north the unit appears more aggradational, as in SU2 and SU3 (Fig. 6). SU4 is situated 33 km more landward than SU3 in the northern sector and 24 km in the southern sector. Laterally subunit 4a is contained in the southern and central sectors, subunits 4b and 4c are distributed extensively across all sectors, tracing two separate along-slope oriented strands.

SU5 has an aggradational stacking pattern resembling that of SU1, it is evenly distributed over the middle slope and increases in thickness on the lower slope (Figs. 11 and 13), unlike the previous units confined to the middle slope.

## 6.2. Evolutionary stages

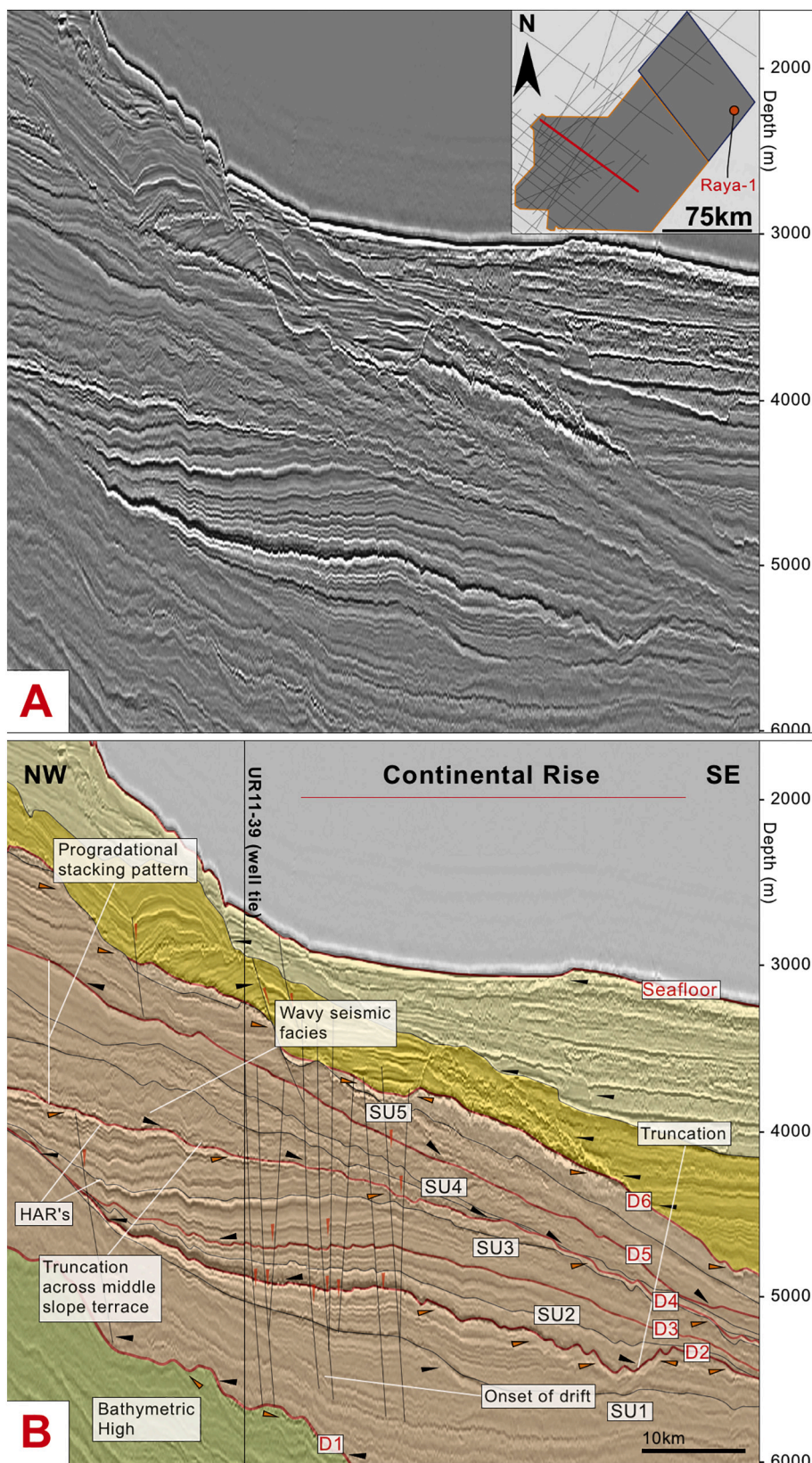
In view of the obtained results, the major changes in the sedimentary stacking pattern and the outlined chronology, the drift can be classified into four broad stages: I) *onset stage*; II) *growth stage*; III) *maintained stage*, and IV) *burial stage*. The first three reflect changes in the depositional system and oceanographic setting of the plastered drift over time, until final burial between the Miocene and the present day sedimentary record.

### 6.2.1. Onset stage (66 Ma – 56 Ma)

The onset stage (SU1) forms a laterally extensive aggradational sheet characterised by low amplitude reflections. The base of the Paleocene (D1) marks a distinct change in the depositional environment, burying the older mixed contourite-turbidite system which formed under the influence of sluggish bottom currents (Creaser et al., 2017). Sediment on the shelf exceeded the Polonio and Plata Highs, thereby allowing for a reconfiguration of river systems that gave rise to the diversion of sediment from the Punta del Este Basin southward, into the Salado Basin (Soto et al., 2011), and northward into the Pelotas Basin. At the same time down-slope processes shut-down, this starved the Punta del Este Basin from the start of the Paleocene (Creaser et al., 2017). This lack of sediment input, particularly in the southern sector, suggests that pelagic sedimentation dominated at this time.

Therefore, the stage stands as part of a long-term pattern that emerged in the wake of marginal domination by gravitational and mixed (down-slope and along-slope) processes (Creaser et al., 2017; Rodrigues et al., 2021). SU1 would represent the beginning of a continental slope dominated by initially weak bottom currents, and the onset of a CDS. By the end of the Paleocene, increasingly erosive discontinuities, and localised aggradation in distal domains point to an expansion of deep-water bottom current activity (Creaser et al., 2017; Hernández-Molina et al., 2018).

During Paleocene times (Fig. 14A) surficial circulation in the South Atlantic resulted from the Upper Pacific Water (UPW) and Agulhas Leakage (Uenzelmann-Neben et al., 2017). The former entered the Atlantic through the Central American Seaway (CAS) and flowed along the South American Margin before deviating eastwards at ~45°S, which continued until ~6 Ma under the partial closing of the CAS, though the Agulhas current still flows into the Atlantic westward from the Indian Ocean (Uenzelmann-Neben et al., 2017). Coevally, one intermediate to deep water mass (Fig. 15A) circulated at depths up to ~2200 m (Via and

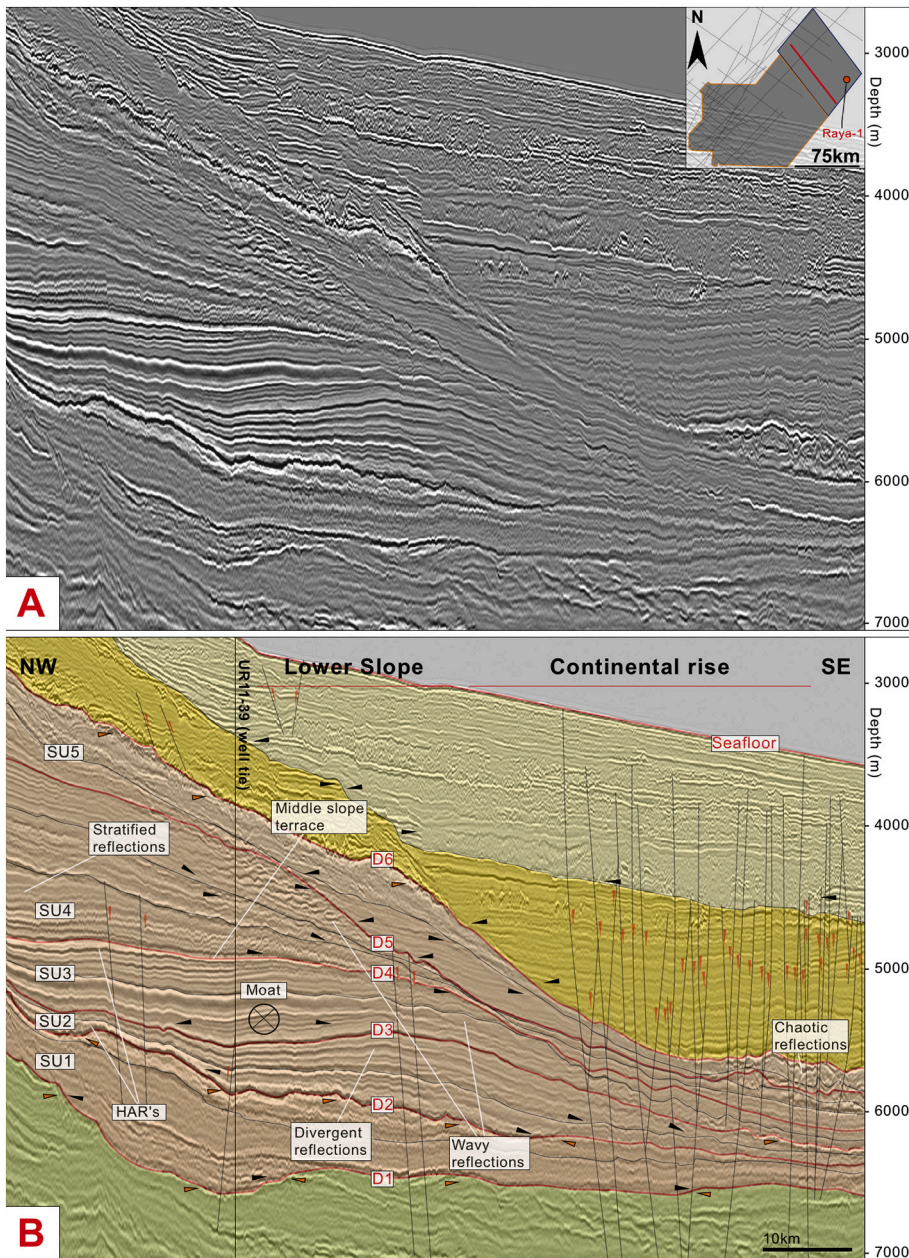


**Fig. 12.** 3D crossline 7600 detailing key seismic observations in the central sector of the studied area, over a bathymetric high. The main seismic units (SU1 to SU5) and discontinuities (D1 to D6) are shown. (courtesy of ANCAP. Original seismic data acquired by BG/Shell). A predominantly aggradational stacking pattern is observed until SU4, which is progradational, yet SU5 appears more aggradational again. Between SU2 and SU4 the units stack landwards, as is clearly observed after the D4 discontinuity, distinctive in the central sector due to increased truncation of SU3 on the middle slope. The onset of drift is clearly identified in high amplitude aggradational parallel and sub-parallel reflections at the top of SU1. D2 is locally more erosive on the rise. The channel is not evident, unlike elsewhere on the margin, the line dissects a relative basement high observed in D2 and D3 in Fig. 7.

Thomas, 2006). It formed in the Weddell Sea and flowed northwards along the South American Margin to ~45°S latitude, where it turned eastward and flowed into the Indian Ocean, achieving weak average velocities of about 5 cm/s (Uenzelmann-Neben et al., 2017). Authors

Batenburg et al. (2018) explain that during the Paleocene the South Atlantic widened and deepened leading to an expansion of deepwater circulation, they state that by ~59 Ma a common deep-water signature could be identified in the South Atlantic, thus indicating increasingly





**Fig. 13.** 3D inline 4400 detailing key seismic observations in the northeast sector. The main seismic units (SU1 to SU5) and discontinuities (D1 to D6) are shown (courtesy of ANCAP. Original data acquired by TOTAL). Within the units, aggradation is predominantly observed against a steep slope. There is subtle evidence of progradation in SU4 and most proximally at the base of SU5, though it is significantly reduced relative to the central and southern sectors, with the units exhibiting a more sheeted configuration. After SU1 the units stack more proximally, which continues to the end of SU4. Intra-unit wavy reflections are observed in SU2; 3 and 4 and HARs are identified associated with D2, D3 and D4. The chaotic reflections pertaining to an MTD on the rise are shown, and the more basinward depocenter described in SU5 is also clearly observed here. Extensive normal faults found across the rise extend through all units, showing minor displacements.

efficient circulation that originated in the Southern Ocean.

The onset of the plastered drift identified along the Uruguayan Margin agrees with the palaeoceanographic setting involving an initially diffuse and weak deep water mass flowing northward with a top boundary (interface) at about 2200 m water depth (Fig. 15A). Enhancement of this water mass towards the end of the Paleocene by early deep waters, caused a focused core localised to distal domains.

#### 6.2.2. Growth stage (Eocene ~56 – ~38 Ma)

The growth stage (SU2 – SU4) began with a major northward depocenter shift from the Punta del Este to the Pelotas Basin, coeval to (and possibly driven by) uplift of the Andean Orogeny, which would have caused flexural subsidence on the margin (Cobbold et al., 2007; Morales et al., 2017; Honegger et al., 2018) (Fig. 11). Sediment transport and deposition were controlled primarily by along-slope processes, with only minor contributions from down-slope processes (Hernández-Molina et al., 2018). The paleoceanographic scenario (Fig. 14B) evolved during the growth stage (Pérez-Díaz and Eagles, 2017), it featured

continuing expansion of deep-water circulation in the Early Eocene (Batenburg et al., 2018) and the possible initiation of a proto-ACC by the Middle Eocene (Uenzelmann-Neben et al., 2017). This configuration was due to greater connectivity between ocean basins in the South Atlantic and gateways in the Southern Ocean (Munday et al., 2015).

During SU2 a relatively low velocity northward flowing core (Fig. 14B), constrained and focused by the morphology of the terrace and the adjacent slope, generated the moat and caused erosion in the southern sector. Sediment was redistributed to distal domains, where along-slope advection produced the subtle mound in northern sector. Bottom currents in the moat may have reached a local velocity of >10 cm/s (Faugères et al., 1999); localised HARs observed within the moat and across erosive discontinuities in the southern sector (see Hernández-Molina et al., 2018) indicate intensified currents (see D2 in Figs. 10 and 12). During SU3, however, bottom currents expanded further, they ran across the middle slope and caused seaward dipping of the terrace, laterally extensive HARs were very prevalent in the central and southern sectors further indicating this bottom current intensification (see Figs. 8,

**Table 5**  
Seismic Subunits.

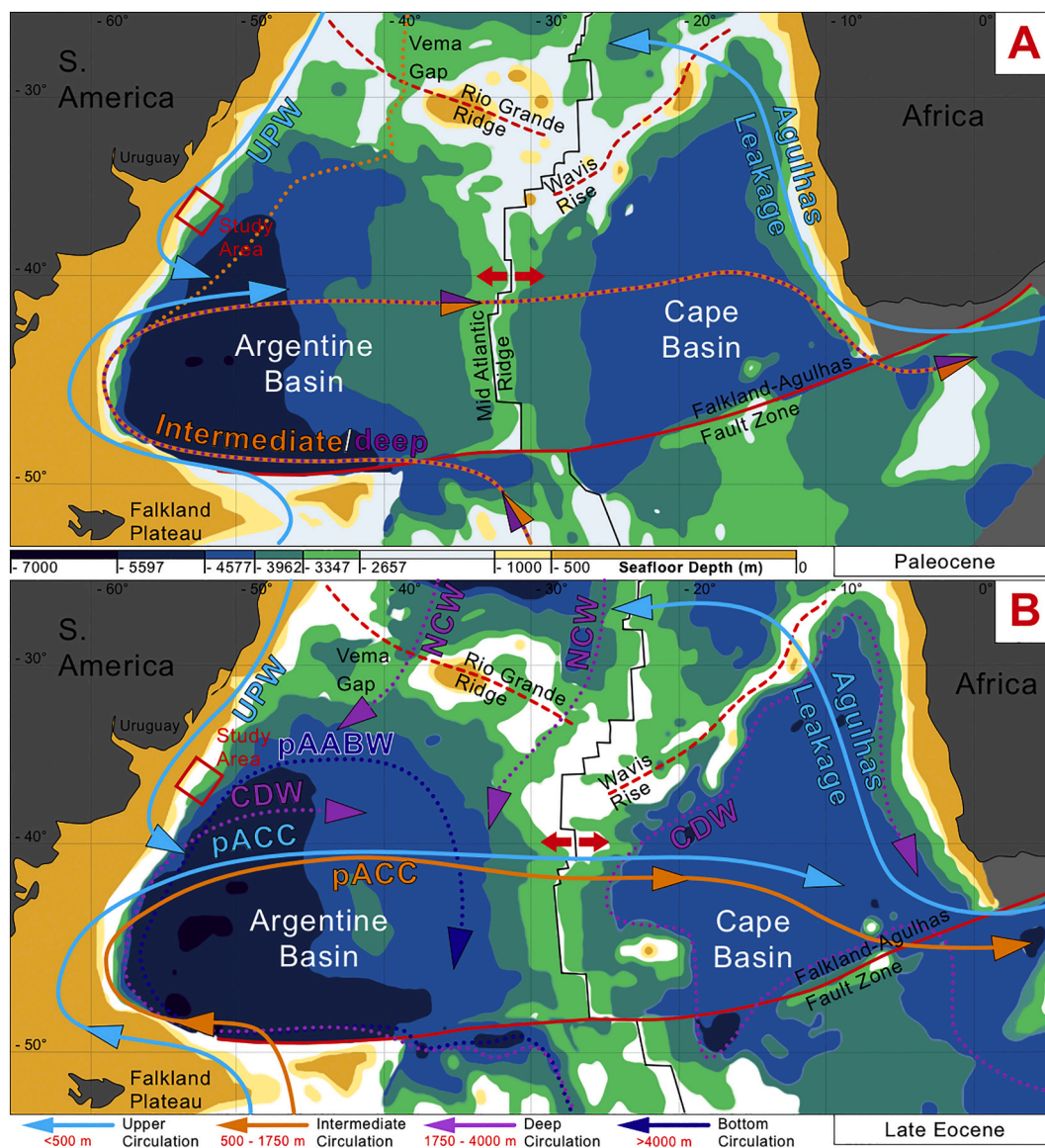
Subunits and Discontinuities	Discontinuity Description	Internal Configuration	Shape
<b>5b</b> d5.1	d5.1 is a regional intermediate amplitude negative discontinuity that is locally erosive on the upper and middle slope	Low to high amplitude parallel, sub parallel, transparent and chaotic reflections that downlap basinwards on the upper slope, onlap landwards and toplap basinwards	Sheet and clinoforms on shelf and upper slope, aggradational sheet on middle slope, lenticular mound on lower slope and sheet on rise
<b>5a</b>		Low to high amplitude parallel, sub parallel, divergent and transparent reflections that onlap D5 proximally, gently downlap distally and toplap basinward	Sheet and clinoforms on shelf and upper slope, aggradational sheet across middle slope, lenticular mounds on lower slope to NE and sheet on rise
<b>4c</b> d4.2	d4.2 is a prominent high amplitude reflection on the lower slope that decreases to low amplitudes proximally, its reflection is highly laterally continuous	Low to high amplitude sub parallel, divergent and wavy reflections on slope, they downlap d4.2 and toplap D5 in a basinward direction. Parallel, transparent and chaotic reflections observed on rise	Lenticular mound to southwest on upper to middle slope, tabular sheet across middle slope that thins in proximal and distal domains
<b>4b</b> d4.1	d4.1 is a low to high amplitude erosive discontinuity that can be observed along the margin on the shelf, slope and rise, it onlaps D4 locally on the lower slope	Low to high amplitude sub parallel, divergent and wavy reflections, they onlap d4.1 landwards on the slope and rise and downlap basinward on the lower slope	Lenticular mound to sheet on upper to middle slope, tabular sheet across middle slope. Thinning is observed towards proximal and distal domains
<b>4a</b>		High to low amplitude parallel, sub parallel and transparent reflections, they onlap D4 landward and to the South and downlap D4 and toplap d4.1 seawards	Lenticular mound on upper to middle slope. Becomes more tabular and sheeted distally and thins on shelf and lower slope
<b>3b</b> d3.1	d3.1 is an intermediate to high amplitude laterally continuous discontinuity that becomes indistinct proximally on the middle slope and to the south of the survey where it onlaps D3	Low to high amplitude parallel and sub parallel reflections, they onlap d3.1 proximally and distally toplap D4 basinward and to the north. 3b becomes progressively truncated to the South	Aggradational sheet on middle slope, showing thinning towards perimeters on upper and lower slope
<b>3a</b>		Low to high amplitude parallel, sub parallel, transparent and wavy reflections. They onlap D3 proximally and onlap and downlap distally. Reflection toplap d3.1 and become truncated distally	Aggradational sheet across middle slope. Thins at depocenter boundaries on upper and lower slope
<b>2b</b> d2.1	d2.1 is a laterally extensive and slightly erosive discontinuity that has a varied reflection profile, it ranges from low to high amplitudes locally	Low to high amplitude sub parallel, divergent and wavy reflections, they onlap d2.1 upslope and downlap d2.1 and toplap D3 basinward	Thin aggradational sheet to southwest, which becomes increasingly mounded to northeast
<b>2a</b>		Intermediate to high amplitude parallel and sub parallel reflections that onlaps D2 landwards, downlap D2 and toplap d2.1 distally	Thin aggradational sheet in southwest thickening and becoming slightly mounded to northeast
<b>1b</b> d1.1	d1.1 is a low to intermediate amplitude discontinuity that is locally erosive, it toplaps D2 on the lower slope to the south of the study area	Internal reflections are intermediate to high amplitude sub parallel and parallel, reflections they onlap the slope landwards and are truncated by D2	Relatively thin aggradational sheeted drape on lower slope
<b>1a</b>		Laterally continuous low to mid amplitude parallel and sub parallel reflections. They onlap D1 proximally and between bathymetric highs and toplap d1.1 landward	Sheeted drape over bathymetry on middle and lower slope that thins on shelf and rise

12 and 13). Then, in SU4, the terrace broadened north-eastwardly, that is, slightly basinward; prograding clinoforms (Honegger et al., 2018) indicate an increased sediment supply likely associated with Andean uplift (Morales et al., 2017). Under the influence of more vigorous bottom currents across the terrace, these sediments were probably partially directed along-slope. All units thin towards the lower slope suggesting little or no deposition, and resulting in a steepening of the

domain.

The retrogradational stacking pattern is a key element of the growth stage. Authors Honegger et al. (2018) linked this to three cycles of base level change. We note that backstepping occurred at the terraces and is most evident in the southern and central sectors (across the terraces of D3 and D4), where erosion is highest (Fig. 13). Recent studies (e.g. Thiéblemont et al., 2019; Miramontes et al., 2020; Rodrigues et al.,



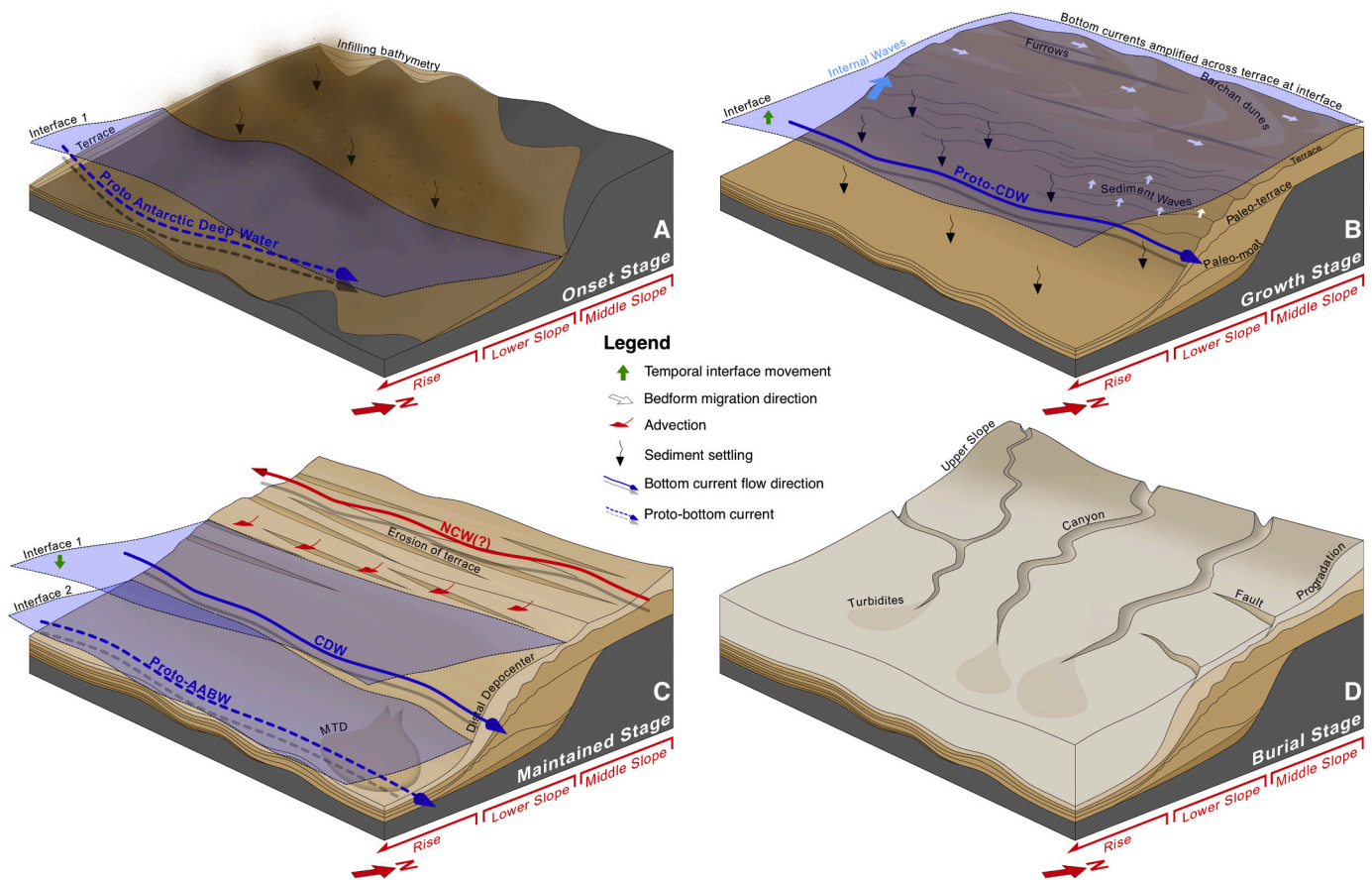


**Fig. 14.** Paleocene (A) and Late Eocene (B) South Atlantic Ocean circulation reconstruction models. Maps, locations and proto-Antarctic Bottom Water (pAABW) adapted from Pérez-Díaz and Eagles (2017). Upper Pacific Water (UPW) and Agulhas Leakage from Uenzelmann-Neben et al. (2017), intermediate/deep water and Circumpolar Deep Water (CDW) inferred from Via and Thomas (2006); Batenburg et al. (2018), proto-Antarctic Circumpolar Current (pACC) inferred from Munday et al. (2015). Water circulation paths are qualitative and arrow length does not indicate current speed; dashed arrows indicate potential circulation depths and paths at the time.

2020) discuss the association of terraces with plastered drifts and the processes modulating their formation; for example, on the margin terraces of Argentina (e.g. Hernández-Molina et al., 2009; Preu et al., 2013); Uruguay (Hernández-Molina et al., 2016); Mozambique (Thiéblemont et al., 2019) and South China (Yin et al., 2019). Along these terraces, the long-term effects of processes related to water mass interfaces (Rebesco et al., 2014) and internal waves/tides induced turbulent energy, causing more erosion and resuspension of sediments (Cacchione et al., 2002; Shanmugam, 2013). Internal solitary waves are known to be common in stratified water columns (LaFond, 1962; Shepard, 1975) and can measure 10's of km in length, tending to have higher amplitudes at intermediate water depths and higher velocities in deep waters (Shanmugam, 2008). Hernández-Molina et al. (2018) explained that the sedimentary succession along the Uruguay slope is controlled by two spatially shifting water masses that evolve over time: an intermediate southward flowing water mass, in conjunction with a northward flowing deep-water mass. The interface of these water masses would have shifted as the water masses themselves evolved spatially and

temporally, which could explain the disposition of the terraces observed in the sequence.

Truncation seen across those terraces and the presence of HARs—as is the case in D2, D3 and D4 (see Figs. 10, 12 and 13)—, are common in plastered drifts, particularly when situated against steeper slopes (Faugères et al., 1999; Rebesco, 2005; Rebesco et al., 2014), and highlight the effects of margin bathymetry on drift evolution. In addition, Hernández-Molina et al. (2018) identified scours, furrows, sand ribbons and 3D barchanoid dunes across the terrace associated with their major discontinuity DIV, which coincides with D4 (Fig. 4). The barchan dunes had a north-eastward (along-slope) migration, thus they are associated with the northward flowing bottom current whose velocity ranged between 0.4 and 1.9 m/s by the end of SU3 (Stow et al., 2009). Furthermore, the current could have been amplified by secondary oceanographic processes, e.g. internal waves/tides (Rebesco et al., 2014; Thran et al., 2018; Yin et al., 2019; Rodrigues et al., 2020). The local erosion observed in our study may have been caused by a spatially varying water mass whose temporally shallowing interface came to



**Fig. 15.** Depositional model depicting key seismic observations and associated sedimentary and oceanographic processes. Bottom current arrows are qualitative and arrow length does not indicate current speed. Dashed arrows indicate potential circulation depths and direction at the time.

modulate drift evolution (Fig. 15B). To the south, a lack of sediment accommodation space beneath the interface might explain increased erosion—these sediments would be eroded and redistributed under the influence of the vigorous currents to less energetic areas. The retrograde stacking pattern reflects the depths at which the interface of the deep-water mass interacted with the slope throughout time (Fig. 15B), meaning the succession could be a relic of the evolving Eocene paleoceanographic circulation.

Oscillations of interfaces by internal waves/tides are commonly considered as a mechanism for generating bedforms (Rebesco et al., 2014). For example, Miramontes et al. (2020) showed that internal waves were responsible for upslope migrating dunes atop a plastered drift on the Mozambican Margin, while Ribó et al. (2016) and Reiche et al. (2018) respectively suggested that such processes played a key role in the generation of sediment waves in the Mediterranean and on the Israeli Margin. In many cases sediment waves are described along the upward termination of terraces (Hernández-Molina et al., 2010; Miramontes et al., 2019; Yin et al., 2019; Rodrigues et al., 2020). Intra-unit landward migrating (WSW) sediment waves are identified on the distal flanks to the north of the study area in SU2 and SU3, and across all sectors in SU4 (see Figs. 8 and 13). They may have been caused by secondary oceanographic processes at the interface propagating perpendicular to the margin, as shown in the Fig. 15B and would thus correspond to a lower energy environment than the more proximal middle slope terrace, as suggested by previous authors (Hernández-Molina et al., 2018; Miramontes et al., 2019; Thiéblemont et al., 2019; Mestdagh et al., 2020), which would periodically encompass the middle slope as it evolves spatially. Similar upslope migrating sedimentary waves were identified by Campbell and Mosher (2016) on the distal flank of the *Shubencadie drift* on the Nova Scotia margin, they suggested

that these waves were controlled by secondary helicoidal flow dynamics or internal waves.

### 6.2.3. Maintained stage (~38 Ma – ~20 Ma)

The maintained stage (SU5) (Fig. 15C) marks a change in the depositional environment, with a low amplitude aggradational sheet seen across the slope (Fig. 5), as previously reported by Morales et al. (2017) and Honegger et al. (2018).

During the maintained stage the CDW (associated with proto-ACC) flowed up the Argentine Margin and deviated eastward at ~45° latitude (Munday et al., 2015; Uenzelmann-Neben et al., 2017). It strengthened by the Late Eocene (~37–35.5 Ma) following a deepening of the Drake's Passage between 41 and 37 Ma, thereby admitting waters at intermediate depths (Fig. 15B) (Sarkar et al., 2019). The proto-AAC thermally isolated the Southern Ocean from warm sub-tropical waters, allowing large-scale ice sheets to form; these ice sheets affected deep-water source regions and gradually enhanced deep circulation (Katz et al., 2011). Around the Late Eocene, the proto-Antarctic Bottom Water (proto-AABW)—possibly initiated and/or enhanced—would have had a lesser density contrast with overlying water masses resulting in slower flows, but possibly similar pathways as at present (Pérez-Díaz and Eagles, 2017). From ~34 Ma (Eocene/Oligocene boundary) onward, the AABW became fully established as a dominant water mass in the Argentine Basin, where it generated large, detached asymmetric mounded drifts on the rise and abyssal plains (Hernández-Molina et al., 2009, 2010, 2016; Gruetzner et al., 2011, 2012; Preu et al., 2012, 2013). Across the slope a relatively weak but efficient proto-CDW persisted until ~32 Ma, when it became more vigorous (Uenzelmann-Neben et al., 2017). This further enhanced deep waters and caused them to deepen during the Oligocene, also affecting the proto-AAIW due to



downwelling, and restricting the coldest Antarctic-sourced waters beneath it. This gave rise to the incursion of the North Atlantic-sourced Northern-Component Water (NCW), a precursor of the NADW, further southward in the Atlantic (Katz et al., 2011). By the Late Oligocene, as suggested by Uenzelmann-Neben et al. (2017), the Atlantic Meridional Overturning Circulation (AMOC) was at work, inferring efficient circulation in the Atlantic, similar to that of the present day. Hernández-Molina et al. (2009) and Gruetzner et al. (2016) noted that intensification of bottom currents in the Oligocene resulted in significant erosion across the Argentine Margin associated with their AR4 discontinuity, which encompassed depths occupied by the Antarctic sourced proto-AAIW, CDW and AABW.

The plastered drift on the Uruguayan Margin shows minor vertical growth, the depocenter shifting to the lower slope, possibly caused by spatial changes in deep waters of the proto-CDW in the Oligocene, and the incursion of the NCW, leading the interface to deepen and limit further growth of the drift (Fig. 15C). The D6 discontinuity shows extensive erosion, truncating SU5 across the slope and rise, in agreement with a deepening and intensifying proto-CDW that largely eroded previous contourite deposits on the margin.

#### 6.2.4. Burial stage (< ~20 Ma)

After D6, the plastered drift became inactive and was buried by younger deposits (Fig. 15D) marking a prominent change in the depositional system during the Neogene. The primary depocenter is cross-cut by down-slope canyons, whose activity along the slope indicates a prominent gravitational influence (Burone et al., 2021). Significant turbidite deposits are observed on the adjacent continental rise (Morales et al., 2017) forming a new depocenter. This increase in basinward sedimentary input could be tied to later stages of Andean uplift affecting the margin (Uenzelmann-Neben et al., 2017), and a coeval fall in sea level further contributed to sediment supply in distal domains via down-slope channels (Hernández-Molina et al., 2018). During the Early Miocene, higher temperatures associated with the climatic optimum resulted in a shallower AMOC than today's (Herold et al., 2012) and weakened the NCW. This permitted the well-established and deepened CDW to move further northwards, increasing its influence in the Argentine Basin (Uenzelmann-Neben et al., 2017). During the Miocene there was a higher influence of the AABW and NADW, as well as greater sediment input (see Hernández-Molina et al., 2009, 2010; Gruetzner et al., 2011, 2012).

### 6.3. Conceptual implications

The plastered drift of this study exhibits a range of sheeted to gently mounded units and a host of secondary erosive and depositional features (e.g. terraces, moats and a variety of bedforms) that, over millions of years, draw a complex CDS affected by two water masses and their respective interface. The drift itself corresponds to the main depositional element, which developed its depocenter where the energy owing to the bottom current from the deeper water mass was minimum. The contourite terrace, in turn, developed on the landward top of the drift, where the energy from the bottom current was maximum. The changes in the sedimentary stacking pattern described for the plastered drift shed light on its lateral and temporal evolution with regards to depositional processes, as well as local and regional bottom current processes and the long-term spatial and temporal changes in water masses and their interfaces.

#### 6.3.1. Margin morphology

The occurrence of large plastered drifts and (associated) flatter terraces modify the morphology of the continental slope completely. Three morphological types (herein Class A, B and C) of slope were recently described by Miramontes et al. (2019); the drift described in this paper evolves through morphological types, this is dependent on the evolution of the depositional environment and oceanographic setting, both

laterally and temporally. Class A outlines a starved margin where vigorous/enhanced bottom currents result in a moat, with the formation of more mounded deposits along-slope, a trend observed at the top of SU1 and in SU2 (Figs. 15 and 16). Class B, in turn, describes a slope with a direct sediment supply swept by a coeval bottom current, resulting in a smoother seafloor with a progradational stacking pattern resembling the one observed in the southern and central sectors during SU4. Class C describes a starved margin with heterogeneous bottom current activity that generates typical plastered drifts across the slope with a convex geometry, as well as mounded features at the base of slope (similar to Type A). A Class C slope most appropriately applies to the drift after SU3 when the margin is affected by multiple water masses (Fig. 15).

#### 6.3.2. Drift types

Rodrigues et al. (2020) recently proposed a model describing three main types of plastered drift (Types 1, 2 and 3) based on lateral and vertical changes in their stacking pattern and observations from the Sines drift on the SW Portuguese Margin: Type 1) a sheeted plastered drift with a lateral erosive or non-depositional terrace; Type 2) a mounded plastered drift with a large V- or U-shaped moat; and Type 3) a tabular, concave plastered drift with a narrow V-shaped moat or valley. They explain that the different types evolve towards each other and towards other drift types. We observed, along the Uruguayan slope, similar characteristics both laterally and temporally. For instance, the drift resembles Type 1 at the top of SU1 and evolves towards Type 2 in SU2, with a proximal along-slope moat. Bathymetry acts as a key control factor, as is evident in the moat—smaller in the south across a shallower slope (Fig. 10), wider and deeper in the north adjacent to a steeper slope (Fig. 13), and replaced by an erosive terrace over bathymetric highs in the central sector (Figs. 12, 16 and 17). From SU3 to SU5 the drift evolves towards Type 1 when the basinward-dipping middle slope terrace is established in all sectors. These subtle alongslope variations in type within the same plastered drift body may be common, highlighting the importance of 3D seismic data for interpreting this system.

#### 6.3.3. Conceptual model for Uruguayan margin plastered drift

The plastered drift on the Uruguayan continental margin (Fig. 17) has a distinctly different geometry between the southern sector, where an adjacent smoother upper slope and increased erosion resulted in a lightly mounded and elongated geometry (e.g. Preu et al., 2013; Hernández-Molina et al., 2018; Thiéblemont et al., 2019), and the northern sector, where a conventional terrace is tied to a convex shape and formed against a steeper slope (e.g. Hernández-Molina et al., 2016; Miramontes et al., 2020). During the growth stage in particular, seismic units are more elongated across the smoother slope in the southern sector, increased erosion could result from amplified bottom currents and secondary oceanographic processes at the water mass interface. The interface would have affected a large area of the smoother seafloor, further contributing to thinner units and owing to the drifts overall elongated geometry (Fig. 7). In the northern sector the seismic units of the growth stage are thicker and more mounded where they are confined against the slope (Fig. 6). Erosion is more constricted as the interface interacts with a smaller area of the steeper seafloor, this combination corresponds to increased accommodation space and owes to the overall convex geometry. The expansion of Antarctic deep waters during the growth stage caused a shallowing of the interface over time, as a result it interacted with the seafloor more proximally and has been preserved in the distinctive retrogradational sedimentary stacking pattern as units of the growth stage step back with the movement of the interface. In SU5 the interface deepens again, eventually resulting in expansive erosion. This model, illustrated in Fig. 17, proposes lateral and temporal changes in the sedimentary stacking pattern and overall drift geometry owing to downcurrent changes in the bottom current behavior, bathymetry, and the variability of long-term water masses through time.

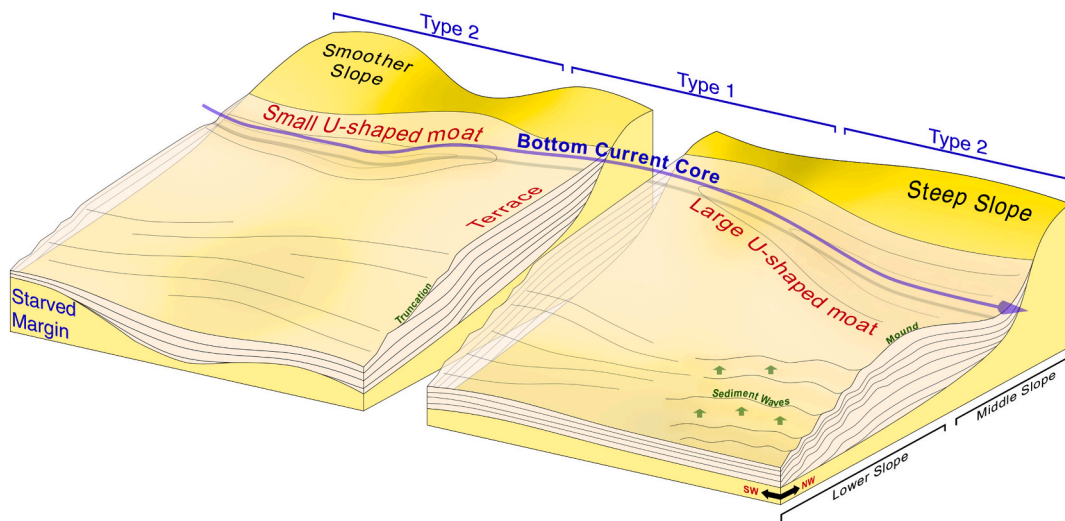


Fig. 16. Model depicting a class A margin after Miramontes et al. (2019), and the key along-slope drift type observed in SU2 after Rodrigues et al. (2020). Bottom current path is qualitative and arrow length does not indicate current speed.

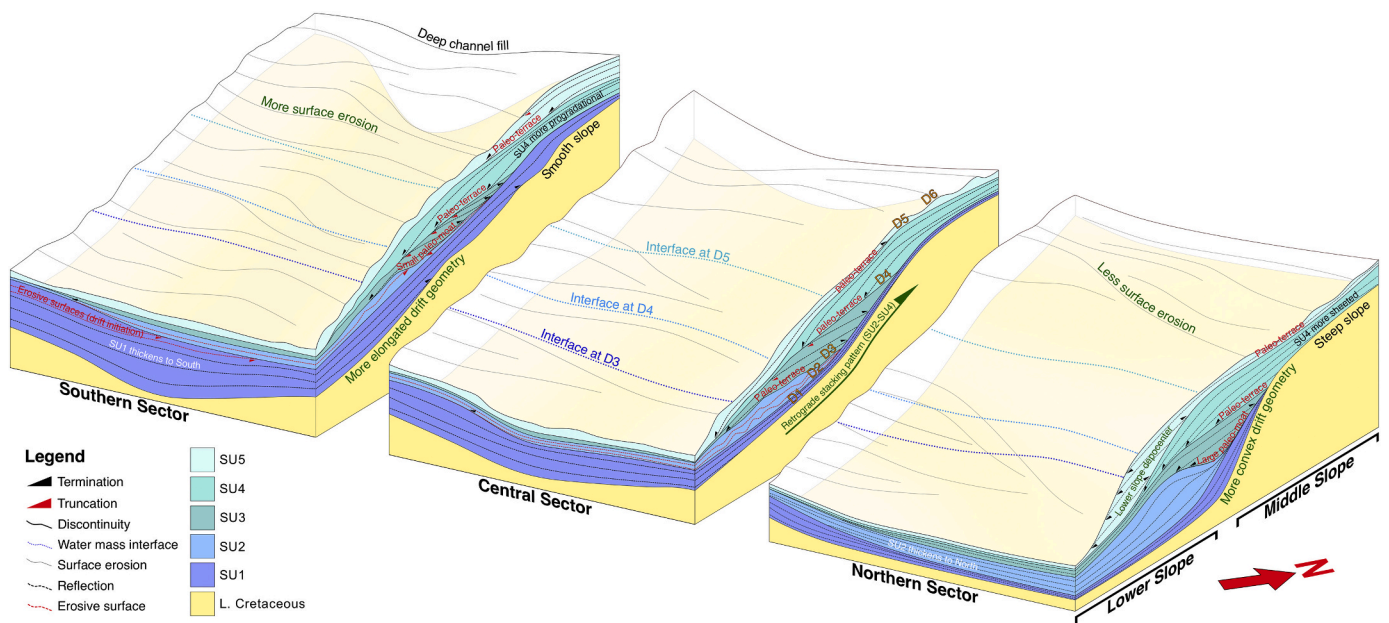


Fig. 17. Sketches displaying, in the southern, central and northern sectors, the key characteristics of the large plastered drifts' lateral and temporal sedimentary stacking pattern, key features identified in the seismic interpretation. The authors envisaged a shallowing of the deep water interface between two water masses from SU1 (dark blue) to SU5 (light blue) during the Growth Stage, resulting in retrogradation. (For interpretation of the references to colour in this figure legend, the reader is referred to the web version of this article.)

7. Conclusion

A large buried Paleogene plastered drift is identified along the Uruguayan continental margin parallel to the middle and lower slope. It is made up of five main seismic units (SU1-SU5) and a number of sub-units subdivided by internal widespread erosive discontinuities, without stratigraphic conformity between the top bounded surfaces of seismic units and their internal layers. The drift itself corresponds to the main depositional element, developing where the bottom currents energy linked to the deeper water mass is minimum. The contourite terrace develops on the landward side of the drift, where the bottom current energy is maximum, and both processes related to the interface and a more vigorous shallower water mass. The drift is associated with terraces, channels, and smaller bedforms (sedimentary waves), denoting a hierarchy of features tied to water mass circulation and interfaces, as

well as further oceanographic processes (i.e. internal waves/tides).

The sedimentary stacking pattern within the plastered drift allowed us to decode four long-term evolutionary stages: I) *Onset Stage* (66 Ma – 56 Ma), whose basal surface represents a prominent erosional surface that marks the onset of drift, and after which extensive sheeted deposits develop; II) *Growth Stage* (Eocene ~ 56 – ~38 Ma), with a prominent landward retrogradational sedimentary stacking pattern (*backstepping*); III) *Maintained Stage* (~38 Ma – ~20 Ma) evidencing limited growth of the drift, and characterised by aggradational sheeted deposits and extensive erosion; and IV) *Burial Stage* (<20 Ma), which determines a major change in the margin evolution, entailing a shift of the main depocenter to deeper domains, thereby resulting in burial of the drift.

The plastered drift formation is attributed to the influence of a deeper water mass, a shallower water mass, and their interface over millions of years. The aforementioned evolutionary stages and the major



changes in the drift depositional style would be a consequence of spatial and vertical changes in the water masses—the Growth Stage for instance, coincided with the expansion and intensification of deep-water circulation that forced a shallowing of its interface, which eventually modulated the formation of the proximal terrace at its top and gave rise to the *backstepping* stacking pattern. Smaller lateral and vertical changes along the seismic units and subunits by the plastered drift reflect local and regional bottom current processes and their interaction with the slope morphology. The slope gradient is a key controlling factor in the lateral bottom current behavior, which could explain the extensive erosion in the southern and central sectors and across bathymetric highs.

This study has further demonstrated the potential of combined 2D and 3D seismic reflection data when characterising the lateral and temporal sedimentary stacking pattern and the evolution of a contouritic drift, as well as for decoding the dominant oceanographic and depositional processes in its long-term formation. The 3D data can demonstrate the more subtle alongslope variations in these complex CDSs, whilst 2D data alone evidently under samples them in many cases. Similar studies are needed to better understand how and when—in geological time—such large contouritic drifts are generated, as they have important implications for basin analysis, paleoceanographic reconstructions, and energy geosciences.

## Dataset

The dataset used in this study is confidential and therefore cannot be made available to the reader.

## Declaration of Competing Interest

The authors declare that they have no known competing financial interests or personal relationships that could have appeared to influence the work reported in this paper.

## Acknowledgements

This study was funded through a Joint Industry Project supported by BP, ENI, ExxonMobil, TOTAL, Wintershall Dea and TGS, within the framework of “The Drifters” Research Group at Royal Holloway University of London (RHUL). Our thanks to ANCAP (*Administración Nacional Combustibles, Alcohol y Portland* – Uruguay) for allowing access to office space, equipment, and all 2D/3D seismic and well data used. Furthermore, thank you to Débora Duarte and Oswaldo Mantilla for aiding in the preparation of surface figures. We would like to thank the editor and the two anonymous reviewers for improving the preliminary submitted manuscript with their positive and detailed suggestions.

## References

- Arhan, M., Naveira-Garabato, A.C., Heywood, K.J., Stevens, D.P., 2002a. The Antarctic circumpolar current between the Falkland Islands and South Georgia. *J. Phys. Oceanogr.* 32, 1914–1931. [https://doi.org/10.1175/1520-0485\(2002\)032<1914:TACCBT>2.0.CO;2](https://doi.org/10.1175/1520-0485(2002)032<1914:TACCBT>2.0.CO;2).
- Alabert, F., Nigretto, G., Dal, J., Marlot, V., Campo, R., Bernard, X., Hardouin, L., Hennuy, J., Jacquelin-Vallee, L., Tarouilly, L., Constant, S., Greenwood, A., Sermondadaz, G., Desegaulx, P., Planus, R., Lesueur, J., Bonnet, L., 2016. *Raya-1 Biostratigraphic Study*. TOTAL.
- Arhan, M., Carton, X., Piola, A., Zenk, W., 2002b. Deep lenses of circumpolar water in the Argentine Basin. *J. Geophys. Res.* 107 (C1), 3007. <https://doi.org/10.1029/2001JC000963>.
- Batenburg, S.J., Voigt, S., Friedrich, O., Osborne, A.H., Bornemann, A., Klein, T., Pérez-Díaz, L., Frank, M., 2018. Major intensification of Atlantic overturning circulation at the onset of Paleogene greenhouse warmth. *Nature* 9, 4954. <https://doi.org/10.1038/s41467-018-07457-7>.
- Burone, L., Franco-Fraguas, P., Carranza, A., Calliari, D., de Mahiques, M.M., Gómez, M., Marin, Y., Gutiérrez, O., Ortega, L., 2021. Physical drivers and dominant oceanographic processes on the Uruguayan margin (Southwestern Atlantic): a review and a conceptual model. *Mar. Sci. Eng.* 9, 304. <https://doi.org/10.3390/jmse9030304>.
- Cacchione, D.A., Pratson, L.F., Ogston, A.S., 2002. The shaping of continental slopes by internal tides. *Science* 296, 724–727. <https://doi.org/10.1126/science.1069803>.
- Campbell, D.C., Mosher, D.C., 2016. Geophysical evidence for widespread Cenozoic bottom current activity from the continental margin of Nova Scotia, Canada. *Mar. Geol.* 378, 237–260. <https://doi.org/10.1016/j.margeo.2015.10.005>.
- Catuneanu, O., Abreu, V., Bhattacharya, J.P., Blum, M.D., Dalrymple, R.W., Eriksson, P. G., Fielding, C.R., Fisher, W.L., Galloway, W.E., Gibling, M.R., Giles, K.A., Holbrook, J.M., Jordan, R., Kendall, C.G.St.C., Macurda, B., Martinsen, O.J., Miall, A.D., Neal, J.E., Nummedal, D., Pomar, L., Posamentier, H.W., Pratt, B.R., Sarg, J.F., Shanley, K.W., Steel, R.J., Strasser, A., Tucker, M.E., Winker, C., 2009. Towards the standardization of sequence stratigraphy. *Earth Sci. Rev.* 92, 1–33. <https://doi.org/10.1016/j.earscirev.2008.10.003>.
- Cobbold, P.R., Rosello, E.A., Roperch, P., Arriagada, C., Gómez, L.A., Cláudio, L., 2007. Distribution, timing, and causes of Andean deformation across South America. In: Ries, A.C., Butler, R.W.H., Graham, R.H. (Eds.), *Deformation of the Continental Crust: The Legacy of Mike Coward*, 272. Geological Society, London, Special Publications, pp. 321–343. <https://doi.org/10.1144/GSL.SP.2007.272.01.17>.
- Combes, V., Matano, R.P., 2014. Trends in the Brazil/Malvinas confluence region. *Geophys. Res. Lett.* 41, 8971–8977. <https://doi.org/10.1002/2014GL062523>.
- Conti, B., de Jesus Perinotto, J.A., Veroslavsky, G., Castillo, M.G., de Santa Ana, H., Soto, M., Morales, E., 2017. Speculative petroleum systems of the Southern Pelotas Basin, offshore Uruguay. *Mar. Pet. Geol.* 83, 1–25. <https://doi.org/10.1016/j.marpetgeo.2017.02.022>.
- Creaser, A., Hernández-Molina, F.J., Badalini, G., Thompson, P., Walker, R., Soto, M., Conti, B., 2017. A late cretaceous mixed (turbidite-contourite) system along the Uruguayan margin: Sedimentary and palaeoceanographic implications. *Mar. Geol.* 390, 234–253. <https://doi.org/10.1016/j.margeo.2017.07.004>.
- Faugères, J.-C., Stow, D.A.V., 1993. Bottom-current-controlled sedimentation: a synthesis of the contourite problem. *Sediment. Geol.* 82, 287–297. [https://doi.org/10.1016/0037-0738\(93\)90127-Q](https://doi.org/10.1016/0037-0738(93)90127-Q).
- Faugères, J.-C., Stow, D.A.V., 2008. Contourite drifts: Nature, evolution and controls. In: Rebesco, M., Camerlenghi, A. (Eds.), *Contourites. Developments in Sedimentology*, 60, pp. 257–288. [https://doi.org/10.1016/S0070-4571\(08\)10014-0](https://doi.org/10.1016/S0070-4571(08)10014-0).
- Faugères, J.-C., Stow, D.A.V., Imbert, P., Viana, A., 1999. Seismic features diagnostic of contourite drifts. *Mar. Geol.* 162, 1–38. [https://doi.org/10.1016/S0025-3227\(99\)00068-7](https://doi.org/10.1016/S0025-3227(99)00068-7).
- Flood, R.D., Shor, A.N., 1988. Mud waves in the Argentine Basin and their relationship to regional bottom circulation patterns. *Deep-Sea Res.* 35, 943–971. [https://doi.org/10.1016/0198-0149\(88\)90070-2](https://doi.org/10.1016/0198-0149(88)90070-2).
- Fonnesu, M., Palermo, D., Galbiati, M., Marchesini, M., Bonamini, E., Bendias, D., 2020. A new world-class deep-water play-type, deposited by the syndepositional interaction of turbidity flows and bottom currents: the giant Eocene Coral Field in northern Mozambique. *Mar. Pet. Geol.* 111, 179–201. <https://doi.org/10.1016/j.marpetgeo.2019.07.047>.
- Franke, D., Neben, S., Schreckenberger, B., Schulze, A., Stiller, M., Krawczyk, C.M., 2006. Crustal structure across the Colorado Basin, offshore Argentina. *Geophysics* 165, 850–864. <https://doi.org/10.1111/j.1365-246X.2006.02907.x>.
- Franke, D., Neben, S., Ladage, S., Schreckenberger, B., Hinz, K., 2007. Margin segmentation and volcano-tectonic architecture along the volcano margin off Argentina/Uruguay, South Atlantic. *Mar. Geol.* 244, 46–67. <https://doi.org/10.1016/j.margeo.2007.06.009>.
- García, M., Hernández-Molina, F.J., Llave, E., Stow, D.A.V., León, R., Fernández-Puga, M. C., Díaz del Río, V., Somoza, L., 2009. Contourite erosive features caused by the Mediterranean Outflow Water in the Gulf of Cadiz: Quaternary tectonic and oceanographic implications. *Mar. Geol.* 257, 24–40. <https://doi.org/10.1016/j.margeo.2008.10.009>.
- Georgi, D.T., 1981. Circulation of bottom water in the southwestern South Atlantic. *Deep-Sea Res.* 28, 959–979. [https://doi.org/10.1016/S0079-6611\(99\)00004-X](https://doi.org/10.1016/S0079-6611(99)00004-X).
- Gordon, A.L., Greengrove, C.L., 1986. Geostrophic circulation of the Brazil-Falkland confluence. *Deep-Sea Res.* 33 (5), 573–585. [https://doi.org/10.1016/0198-0149\(86\)90054-3](https://doi.org/10.1016/0198-0149(86)90054-3).
- Gruetznher, J., Uenzelmann-Neben, G., Franke, D., 2011. Variations in bottom water activity at the Southern Argentine margin: indications from a seismic analysis of a continental slope terrace. *Geo-Mar. Lett.* 31, 405–417. <https://doi.org/10.1007/s00367-011-0252-0>.
- Gruetznher, J., Uenzelmann-Neben, G., Franke, D., 2012. Variations in sediment transport at the central Argentine continental margin during the Cenozoic. *Geochem. Geophys. Geosyst.* 13, 10. <https://doi.org/10.1029/2012GC004266>.
- Gruetznher, J., Uenzelmann-Neben, G., Franke, D., 2016. Evolution of the northern Argentine margin during the Cenozoic controlled by bottom current dynamics and gravitational processes. *Geochem. Geophys. Geosyst.* 17, 3131–3149. <https://doi.org/10.1002/2015GC006232>.
- Haq, B.U., Hardenbol, J., Vail, P.R., 1987. Chronology of fluctuating sea levels since the triassic. *Science* 235, 1156–1167. <https://doi.org/10.1126/science.235.4793.1156>.
- Hernández-Molina, F.J., Llave, E., Somoza, L., Fernández-Puga, M.C., Maestro, A., León, R., Barnolas, A., Medialdea, T., García, M., Díaz del Río, V., Fernández-Salas, L. M., Vázquez, J.T., Lobo, F., Alveirinho Dias, J.M., Rodero, J., Gardner, J., 2003. Looking for clues to paleoceanographic imprints: a diagnosis of the Gulf of Cadiz contourite depositional systems. *Geology* 31 (1), 19–22. [https://doi.org/10.1130/0091-7613\(2003\)031<0019:LFCTPI>2.0.CO;2](https://doi.org/10.1130/0091-7613(2003)031<0019:LFCTPI>2.0.CO;2).
- Hernández-Molina, F.J., Llave, E., Stow, D.A.V., García, M., Somoza, L., Vázquez, J.T., Lobo, F.J., Maestro, A., Díaz del Río, V., León, R., Medialdea, T., Gardner, J., 2006. The contourite depositional system of the Gulf of Cadiz: a sedimentary model related to the bottom current activity of the Mediterranean outflow water and its interaction with the continental margin. *Deep-Sea Res. Part II* 53, 1420–1463. <https://doi.org/10.1016/j.dsr2.2006.04.016>.

- Hernández-Molina, F.J., Llave, E., Stow, D.A.V., 2008a. Continental slope contourites. In: Rebesco, M., Camerlenghi, A. (Eds.), *Contourites. Developments in Sedimentology*, 60, pp. 379–408. [https://doi.org/10.1016/S0070-4571\(08\)10019-X](https://doi.org/10.1016/S0070-4571(08)10019-X).
- Hernández-Molina, F.J., Maldonado, A., Stow, D.A.V., 2008b. Abyssal plain contourites. In: Rebesco, M., Camerlenghi, A. (Eds.), *Contourites. Developments in Sedimentology*, 60, pp. 345–378. [https://doi.org/10.1016/S0070-4571\(08\)10018-8](https://doi.org/10.1016/S0070-4571(08)10018-8).
- Hernández-Molina, F.J., Paterlini, M., Violante, R., Marshall, P., de Isasi, M., Somoza, L., Rebesco, M., 2009. Contourite depositional system on the argentine slope: an exceptional record of the influence of Antarctic water masses. *Geology* 37 (6), 507–510. <https://doi.org/10.1130/G25578A.1>.
- Hernández-Molina, F.J., Paterlini, M., Somoza, L., Violante, R., Arecco, M.A., de Isasi, M., Rebesco, M., Uenzelmann-Neben, G., Neben, S., Marshall, P., 2010. Giant mounded drifts in the argentine Continental margin: Origins, and global implications for the history of thermohaline circulation. *Mar. Pet. Geol.* 27, 1508–1530. <https://doi.org/10.1016/j.marpetgeo.2010.04.003>.
- Hernández-Molina, F.J., Soto, M., Piola, A.R., Tomasini, J., Preu, B., Thompson, P., Badalini, G., Creaser, A., Violante, R.A., Morales, E., Paterlini, M., de Santa Ana, H., 2016. A contourite depositional system along the Uruguayan continental margin: Sedimentary, oceanographic and paleoceanographic implication. *Mar. Geol.* 378, 333–349. <https://doi.org/10.1016/j.margeo.2015.10.008>.
- Hernández-Molina, F.J., Campbell, S., Badalini, G., Thompson, P., Walker, R., Soto, M., Conti, B., Preu, B., Thiéblemont, A., Hyslop, L., Miramontes, E., Morales, E., 2018. Large bedforms on contourite terraces: Sedimentary and conceptual implications. *Geology* 46 (1), 27–30. <https://doi.org/10.1130/G39655.1>.
- Herold, N., Huber, M., Müller, R.D., Seton, M., 2012. Modeling the Miocene climatic optimum: Ocean circulation. *Paleoceanography* 27, PA1209. <https://doi.org/10.1029/2010PA002041>.
- Hinz, K., Neben, S., Schreckenberger, B., Roeser, H.A., Block, M., Goncalves de Souza, K., Meyer, H., 1999. The argentine continental margin north of 48°S: Sedimentary successions, volcanic activity during breakup. *Mar. Pet. Geol.* 16, 1–25. [https://doi.org/10.1016/S0264-8172\(98\)00060-9](https://doi.org/10.1016/S0264-8172(98)00060-9).
- Honegger, B.V., Morales, E., Soto, M., Conti, B., 2018. Seismic stratigraphy of the eocene-lower oligocene in the uruguayan continental margin. *J. Sediment. Environ.* 3 (4), 290–306. <https://doi.org/10.12957/jse.2018.39248>.
- Katz, M.E., Cramer, B.S., Toggweiler, J.R., Esmay, G., Liu, C., Miller, K.G., Rosenthal, Y., Wade, B.S., Wright, J.D., 2011. Impact of antarctic circumpolar current development on late paleogene ocean structure. *Science* 332, 1076–1079. <https://doi.org/10.1126/science.1202122>.
- LaFond, E.C., 1962. Internal waves. In: Hill, M.N. (Ed.), *The Sea*, 1. Wiley-Interscience, New York, pp. 731–751. <https://doi.org/10.1002/j.2161-4296.1962.tb02523.x>.
- Lofi, J., Voelker, A.H.L., Ducassou, E., Hernández-Molina, F.J., Sierro, F.J., Bahr, A., Galvani, A., Lourens, L.J., Pardo-Igúzquiza, E., Pezard, P., Rodríguez-Tovar, F.J., Williams, T., 2016. Quaternary chronostratigraphic framework and sedimentary processes for the Gulf of Cadiz and Portuguese Contourite Depositional Systems derived from Natural Gamma Ray records. *Mar. Geol.* 377, 40–57. <https://doi.org/10.1016/j.margeo.2015.12.005>.
- McCave, I.N., Tucholke, B.E., 1986. Deep current-controlled sedimentation in the western North Atlantic. In: Vogt, P.R., Tucholke, B.E. (Eds.), *The Geology of North America: The Western North Atlantic Region*, M, pp. 451–468. <https://doi.org/10.1130/DNAG-GNA-M.451>.
- Mestdagh, T., Lobo, F.J., Llave, E., Hernández-Molina, F.J., Ledesma, A.G., Puga-Bernábeu, A., Fernández-Salas, L.-M., Van Rooij, D., 2020. Late Quaternary multi-genetic processes and products of the northern Gulf of Cadiz upper continental slope (SW Iberian Peninsula). *Mar. Geol.* 427, 106214. <https://doi.org/10.1016/j.margeo.2020.106214>.
- Miller, K.G., Kominz, M.A., Browning, J.V., Wright, J.D., Mountain, G.S., Katz, M.E., Sugarman, P.J., Cramer, B.S., Christie-Blick, N., Pekar, S.F., 2005. The phanerozoic record of global sea-level change. *Science* 310, 1293–1298. <https://doi.org/10.1126/science.1116412>.
- Miramontes, E., Garreau, P., Caillaud, M., Jouet, G., Pellen, R., Hernández-Molina, F.J., Clare, M.A., Cattaneo, A., 2019. Contourite distribution and bottom currents in the NW Mediterranean Sea: Coupling seafloor geomorphology and hydrodynamic modelling. *Geomorphology* 333, 43–60. <https://doi.org/10.1016/j.geomorph.2019.02.030>.
- Miramontes, E., Jouet, G., Thereau, E., Bruno, M., Penven, P., Guerin, C., le Roy, P., Droz, L., Jorry, S.J., Hernández-Molina, F.J., Thiéblemont, A., Jacinto, R.S., Cattaneo, A., 2020. The impact of internal waves on upper continental slopes: insights from the Mozambican margin (Southwest Indian Ocean). *Earth Surf. Process. Landf.* 45, 1469–1482. <https://doi.org/10.1002/esp.4818>.
- Mitchum Jr., R.M., Vail, P.R., Sangree, S.J., 1977. Seismic stratigraphy and global changes of sea level, part 6: stratigraphic interpretation of seismic reflection patterns in depositional sequences. In: Payton, C.E. (Ed.), *Seismic Stratigraphy – Applications to Hydrocarbon Exploration*, 26. AAPG Memoirs, pp. 117–133.
- Morales, E., 2013. *Evolução Tectónica e Estratigráfica das Bacias da Margem Continental do Uruguai. Tese de Doutorado, Universidade Estadual Paulista*.
- Morales, E., Chang, H.K., Soto, M., Corrêa, F.S., Veroslavsky, G., de Santa Ana, H., Conti, B., Daners, G., 2017. Tectonic and stratigraphic evolution of the Punta del Este and Pelotas basins (offshore Uruguay). *Pet. Geosci.* 23, 415–426. <https://doi.org/10.1144/petgeo2016-059>.
- Munday, D.R., Johnson, H.L., Marshall, D.P., 2015. The role of ocean gateways in the dynamics and sensitivity to wind stress of the early Antarctic Circumpolar current. *Paleoceanography* 30, 284–302. <https://doi.org/10.1002/2014PA002675>.
- Nielsen, T., Kuijpers, A., Knutz, P., 2008. Seismic expression of contourite depositional systems. In: Rebesco, M., Camerlenghi, A. (Eds.), *Contourites. Developments in Sedimentology*, 60, pp. 301–322. [https://doi.org/10.1016/S0070-4571\(08\)10016-4](https://doi.org/10.1016/S0070-4571(08)10016-4).
- Pérez-Díaz, L., Eagles, G., 2014. Constraining South Atlantic growth with seafloor spreading data. *Tectonics* 33, 1848–1873. <https://doi.org/10.1002/2014TC003644>.
- Pérez-Díaz, L., Eagles, G., 2017. South Atlantic paleobathymetry since early cretaceous. *Sci. Rep.* 7. <https://doi.org/10.1038/s41598-017-11959-7>, 11819–16.
- PGS, 2014. *Data Processing Report – Blocks 8, 9 and 13 Offshore Uruguay for BG Uruguay. Processing Project no 3255bg. January 2013–September 2014*.
- Piola, A.R., Matano, R.P., 2001. *The South Atlantic Western Boundary Currents Brazil/Falkland (Malvinas) Currents*. In: Steele, J.H. (Ed.), *Encyclopedia of Ocean Sciences*, London, Academic Press, vol. 1, pp. 340–349.
- Preu, B., Schwenk, T., Hernández-Molina, F.J., Violante, R., Paterlini, M., Krastel, S., Tomasini, J., Spieß, V., 2012. Sedimentary growth pattern on the northern argentine slope: the impact of North Atlantic Deep Water on southern hemisphere slope architecture. *Mar. Geol.* 329–331, 113–125. <https://doi.org/10.1016/j.margeo.2012.09.009>.
- Preu, B., Hernández-Molina, F.J., Violante, R., Piola, A.R., Paterlini, C.M., Schwenk, T., Voigt, I., Krastel, S., Spieß, V., 2013. Morphosedimentary and hydrographic features of the northern argentine margin: the interplay between erosive, depositional and gravitational processes and its conceptual implications. *Deep-Sea Res.* 75, 157–174. <https://doi.org/10.1016/j.dsr.2012.12.013>.
- Rebesco, M., 2005. Contourites. In: Selley, R.C., Cocks, L.R.M., Plimer, I.R. (Eds.), *Encyclopedia of Geology*, 4. Elsevier, Oxford, pp. 513–527. <https://doi.org/10.1016/B0-12-369396-9/00497-4>.
- Rebesco, M., Camerlenghi, A. (Eds.), 2008. *Dev. Sedimentol.* 60, 1–663.
- Rebesco, M., Stow, D.A.V., 2001. Seismic expression of contourites and related deposits: a preface. *Mar. Geophys. Res.* 22, 303–308. <https://doi.org/10.1023/A:1016316913639>.
- Rebesco, M., Hernández-Molina, F.J., van Rooij, D., Wåhlin, A., 2014. Contourites and associated sediments controlled by deep-water circulation processes: State-of-the-art and future considerations. *Mar. Geol.* 352, 111–154. <https://doi.org/10.1016/j.margeo.2014.03.011>.
- Reiche, S., Hübscher, C., Brenner, S., Betzler, C., Hall, J.K., 2018. The role of internal waves in the late Quaternary evolution of the Israeli continental slope. *Mar. Geol.* 406, 177–192. <https://doi.org/10.1016/j.margeo.2018.09.013>.
- Ribó, M., Puig, P., Muñoz, A., Lo Iacono, C., Masqué, P., Planques, A., Acosta, J., Guillén, J., Ballesteros, M.G., 2016. Morphobathymetric analysis of the large fine-grained sediment waves over the Gulf of Valencia continental slope (NW Mediterranean). *Geomorphology* 253, 22–37. <https://doi.org/10.1016/j.geomorph.2015.09.027>.
- Rodrigues, S., Roque, C., Hernández-Molina, F.J., Llave, E., Terrinha, P., 2020. The sines contourite depositional system along the SW Portuguese margin: Onset, evolution and conceptual implications. *Mar. Geol.* 430, 106357. <https://doi.org/10.1016/j.margeo.2020.106357>.
- Rodrigues, S., Hernández-Molina, F.J., Kirby, A., 2021. A late cretaceous hybrid (turbidite-contourite) system along the argentine margin: Paleoceanographic and conceptual implications. *Mar. Pet. Geol.* 123, 104768. <https://doi.org/10.1016/j.marpetgeo.2020.104768>.
- Sarkar, S., Basak, C., Frank, M., Berndt, C., Huuse, M., Badhani, S., Bialas, J., 2019. Late eocene onset of the proto-antarctic circumpolar current. *Sci. Rep.* 9. <https://doi.org/10.1038/s41598-019-46253-1>, 10125–10.
- Shanmugam, G., 2008. Deep-water bottom currents and their deposits. In: Rebesco, M., Camerlenghi, A. (Eds.), *Contourites. Developments in Sedimentology*, 60, pp. 59–81. [https://doi.org/10.1016/S0070-4571\(08\)10005-X](https://doi.org/10.1016/S0070-4571(08)10005-X).
- Shanmugam, G., 2013. Modern internal waves and internal tides along oceanic pycnoclines: challenges and implications for ancient deep-marine baroclinic sands. *AAPG Bull.* 97 (5), 799–843. <https://doi.org/10.1306/10171212101>.
- Shepard, F.P., 1975. Progress of internal waves along submarine canyons. *Mar. Geol.* 19 (3), 131–138. [https://doi.org/10.1016/0025-3227\(75\)90065-1](https://doi.org/10.1016/0025-3227(75)90065-1).
- Soto, M., Morales, E., Veroslavsky, G., de Santa Ana, H., Ucha, N., Rodríguez, P., 2011. The continental margin of Uruguay: Crustal architecture and segmentation. *Mar. Pet. Geol.* 28, 1676–1689. <https://doi.org/10.1016/j.marpetgeo.2011.07.001>.
- Stokes, F.A., Campbell, C.V., Cass, R., Ucha, N., 1991. Seismic stratigraphic analysis of the Punta Del Este Basin, offshore Uruguay, South America. *Am. Assoc. Pet. Geol. Bull.* 75 (2), 219–240. <https://doi.org/10.1306/0C9B278B-1710-11D7-8645000102C1865D>.
- Stow, D.A.V., Faugères, J.-C., Howe, J.A., Pudsey, C.J., Viana, A.R., 2002. Bottom currents, contourites and deep-sea sediment drifts: Current state-of-the-art. In: Stow, D.A.V., Pudsey, C.J., Howe, J.A., Faugères, J.-C., Viana, A.R. (Eds.), *Deep-Water Contourite Systems: Modern Drifts and Ancient Series, Seismic and Sedimentary Characteristics*, vol. 22. Geological Society of London Memoirs, pp. 7–20. <https://doi.org/10.1144/GSL.MEM.2002.022.01.02>.
- Stow, D.A.V., Hernández-Molina, F.J., Llave, E., Sayago-Gil, M., Díaz-del Río, V., Branson, A., 2009. Bedform-velocity matrix: the estimation of bottom current velocity from bedform observations. *Geology* 37, 327–330. <https://doi.org/10.1130/G25259A.1>.
- Stramma, L., England, M., 1999. On the water masses and mean circulation of the South Atlantic Ocean. *J. Geophys. Res.* 104, 20863–20883. <https://doi.org/10.1029/1999JC900139>.
- Sun, Q., Cartwright, J., Lüdmann, T., Wu, S., Yao, G., 2017. Three-dimensional characterization of a complex sediment drift in the South China Sea: evidence for unsteady flow regime. *Sedimentology* 64 (3), 832–853. <https://doi.org/10.1111/sed.12330>.
- Thiéblemont, A., Hernández-Molina, F.J., Miramontes, E., Raison, F., Penven, P., 2019. Contourite depositional systems along the Mozambique Channel: the interplay



- between bottom currents and sedimentary processes. *Deep-Sea Res.* 147, 79–99. <https://doi.org/10.1016/j.dsr.2019.03.012>.
- Thiéblemont, A., Hernández-Molina, F.J., Ponte, J.-P., Robin, C., Guillocheau, F., Gazzola, C., Raison, F., 2020. Seismic stratigraphic framework and depositional history for cretaceous and Cenozoic contourite depositional systems of the Mozambique Channel, SW Indian Ocean. *Mar. Geol.* 425, 106192. <https://doi.org/10.1016/j.margeo.2020.106192>.
- Thran, A.C., Dutkiewicz, A., Spence, P., Müller, R.D., 2018. Controls on the global distribution of contourite drifts: Insights from an eddy-resolving ocean model. *Earth Planet. Sci. Lett.* 489, 228–240. <https://doi.org/10.1016/j.epsl.2018.02.044>.
- Tozer, B., Sandwell, D.T., Smith, W.H.F., Olson, C., Beale, J.R., Wessel, P., 2019. Global bathymetry and topography at 15 arc seconds: SRTM15+. *Earth Space Sci.* 6, 1847–1864. <https://doi.org/10.1029/2019EA000658>.
- Uenzelmann-Neben, G., Weber, T., Grützner, J., Thomas, M., 2017. Transition from the cretaceous ocean to Cenozoic circulation in the western South Atlantic – a twofold reconstruction. *Tectonophysics* 716, 225–240. <https://doi.org/10.1016/j.tecto.2016.05.036>.
- Valla, D., Piola, A.R., Meinen, C.S., Campos, E., 2018. Strong mixing and recirculation in the Northwestern Argentine Basin. *J. Geophys. Res. Oceans* 123, 4624–4648. <https://doi.org/10.1029/2018JC013907>.
- Via, R.K., Thomas, D.J., 2006. Evolution of the Atlantic thermohaline circulation: early Oligocene onset of deep-water production in the North Atlantic. *Geology* 34 (6), 441–444. <https://doi.org/10.1130/G22545.1>.
- Viana, A.R., 2008. Economic relevance of contourites. In: Rebesco, M., Camerlenghi, A. (Eds.), *Contourites. Developments in Sedimentology*, 60, pp. 493–510. [https://doi.org/10.1016/S0070-4571\(08\)10023-1](https://doi.org/10.1016/S0070-4571(08)10023-1).
- Yin, S., Hernández-Molina, F.J., Zhang, W., Li, J., Wang, L., Ding, W., Ding, W., 2019. The influence of oceanographic processes on contourite features: a multidisciplinary study of the northern South China Sea. *Mar. Geol.* 415, 105967. <https://doi.org/10.1016/j.margeo.2019.105967>.